Microscopic quasiparticle-phonon model in the study of the beta decay of Cd-115

Mikko Haaranen

UNIVERSITY OF JYVÄSKYLÄ

Master's Thesis
University of Jyväskylä, Department of Physics
24.1.2013
Supervisor: Jouni Suhonen

Preface

This Master's thesis, which I wrote during the summer and autumn semester of 2012, is the very apex to my nearly five years of studies at the Department of Physics of the University of Jyväskylä. I would like to thank my supervisor, Professor Jouni Suhonen for this interesting choice of topic. I already had the great opportunity to write my Bachelor's thesis under his experienced guidance during the summer of 2011.

I also wish to thank Ph.D. Mika Mustonen and Ph.D. Emanuel Ydrefors for the computer codes they provided for the use of this work. Mika deserves my graditude also for his patient guidance in all the practical matters at the beginning of my 2011 summer project.

Furthermore, I would like to thank all my friends and relatives for their support. I wish them all the best.

Abstract

This master's thesis concerns the use of the microscopic quasiparticle-phonon model in the study of the β^- decay of ^{115}Cd. The first part of this text concentrates on the theoretical description of nearly spherical open-shell odd-A nuclei by using the microscopic quasiparticle-phonon model. The treatment of the subject is far from exhaustive but all the necessary relations needed in the practical application of the formalism are provided in the text.

The second part provides the theory that is needed for the study of β^- decay. In addition to the general theory of forbidden β^- decay, also the greatly simplified case of allowed transitions are discussed. Again rather than providing a fully comprehensive treatment of the subject, a more streamlined approach is adopted. All the various relations that are needed in the practical application of the theory are provided in the text.

Finally, in the third and final part of the text the above theoretical framework is applied to the β^- decay of ^{115}Cd. In addition to the ground state transitions of ^{115}Cd, it is also possible to study the transitions coming from the first excitation state due to its isomeric character. Because of the various possible ways of carrying out the fitting of the QRPA phonons, several sets of calculated partial half-lives are obtained. The calculated partial half-lives are compared to experimental results. For several transitions values that are fairly close to the experimental ones can be found. However, in many cases there are large disrepancies between the two. Some of the transitions seem also to be very sensitive to the adjustments made to the QRPA phonons. The effect of varying the nucleon spin-orbit interaction strength was studied as an additional exercise.

Contents

Introduction

The theory of nuclear beta decay has gained a well established position in today's nuclear physics. Thanks to its success in accurately describing the most typical beta transitions, the theory itself is not usually regarded worth active study anymore. Despite being a somewhat unfashionable subject, the beta decay theory is still a good test bench for nuclear models. The kinematic part of the theory is fully universal but the charge-changing transition densities (CCTDs) inside the nuclear matrix elements are not. These quantities carry the nuclear structure information and in order to calculate them an actual nuclear model must be specified.

A fully microscopic example of such a nuclear model, and the one that is used in this text, is the microscopic quasiparticle-phonon model (MQPM) for nearly spherical odd-A open shell nuclei [1]. The starting point for using this formalism is to choose a even-even nucleus that is used as a reference nucleus. To lighten the involved computational burden, the configuration space of the reference nucleus is divided into two parts [2]. The innermost nuclear orbitals form an inert nuclear core and only the outer orbitals contribute to the interactions that lead to the formation of the excited states of the nucleus. The collection of these active outer nuclear orbitals of the reference nucleus is called the valence space.

The ground state of the reference nucleus can be obtained from the BCS theory [1,2]. In the BCS theory the basic constituents of nuclei are not particles or holes but rather quasiparticles that have both particle and hole components. The ground and excited states of the neighbouring odd-A nuclei can then be descriped as one-quasiparticle excitations on top of the ground state of the reference nucleus. The one-quasiparticle description can be considerably improved by introducing the MQPM three-quasiparticle excitations. These three-quasiparticle excitations are constructed by combining the BCS one-quasiparticle states with the QRPA two-quasiparticle states [1]. The QRPA two-quasiparticle excitations are considered to be the basic excitations of the even-even reference nucleus.

1 Theoretical description of nuclear states

In this section the needed theoretical framework that is used to describe the different nuclear states of an open-shell odd-A nucleus is developed. The starting point for the discussion is the nuclear mean-field potential that leads to the discrete set of single-particle states.

The nuclear model based directly on the consept of these single-particle orbitals is the mean-field shell model [2]. Despite the fact that the mean-field shell model correctly predicts at least some of the low-energy states of nearly magic nuclei[1], it is not applicable to open-shell nuclei with several nucleons above a fully closed major shell. To overcome the challenges faced with the open-shell nuclei, one must strive for a more refined model. The starting point for this is the BCS theory and the introduction of the BCS quasiparticles [1].

1.1 Nuclear mean field and Woods–Saxon potential

The many-particle problem of A strongly interacting nucleons is described by a nuclear Hamiltonian $H = T+V$ [2]. The kinetic-energy term T is a simple sum of the kinectic energies of the individual nucleons. The potential-energy term V holds the potential energies of the interactions between the different pairs of nucleons and has therefore a more complicated two-body character. By introducing a new mean-field potential with the additional potential energies of the individual nucleons summed to a term V_{MF}, it is now possible to write the nuclear Hamiltonian in a form

$$H = [\, T + V_{\mathrm{MF}} \,] + [\, V - V_{\mathrm{MF}} \,] = H_{\mathrm{MF}} + V' \,, \quad H_{\mathrm{MF}} = \sum_{i=1}^{A} h_i \,. \tag{1}$$

If the latter part V', the residual interactions containing all the two-body interactions, is now effectively enough suppressed by maximizing the first part, namely H_{MF}, it can be treated as a small perturbation. This procedure of effectively replacing the A strongly interacting nucleons with weakly interacting mean-field quasiparticles is the nuclear mean-field approximation [2].

There is a procedure of obtaining a proper mean-field potential via the iterative use of Hartree–Fock equation, but more common is simply to choose a suitable phenomenological potential (see for example the discussion in [2]). An example of such a phenomenological potential with realistic nuclear mean-field behaviour is the Woods–Saxon potential

$$v_{\mathrm{WS}}(r) = -\frac{V_0}{1 + e^{(r-R)/a}} \tag{2}$$

that is used in the discussion of this text [2]. With the usual parametrization, the nuclear radius R and the surface diffuseness a are taken to be

$$R = 1.27 A^{1/3}\,\mathrm{fm}\,, \quad a = 0.67\,\mathrm{fm}. \tag{3}$$

The depth V_0 of the potential is chosen according to the relation

$$V_0 = \left(51 \pm 33 \frac{N-Z}{A} \right) \mathrm{MeV}, \tag{4}$$

1. Nearly magic nuclei have few nucleons (nucleon holes) above (below) a fully closed major shell at some magic number.

where the result with + sign is selected for protons and the result with − sign for neutrons.

When the Coulomb interaction and the spin-orbit interaction are also taken into account, the complete single-particle Hamiltonian that already formally appeared in (1), can now be written as [2]

$$h = -\frac{\hbar^2}{2m_N}\nabla^2 + v_{\mathrm{WS}}(r) + v_{\mathrm{C}}(r) + v_{\mathrm{LS}}(r)\vec{L}\cdot\vec{S} \tag{5}$$

In this text the same nucleon mass $m_N = 940\,\mathrm{MeV/c^2}$ is used for both protons and neutrons. The Coulombic potential energy $v_{\mathrm{C}}(r)$ that is needed only for protons is taken to be

$$v_{\mathrm{C}}(r) = \frac{Ze^2}{4\pi\epsilon_0}\begin{cases} \frac{3-(r/R)^2}{2R}, & r \le R \\ \frac{1}{r}, & r > R \end{cases} . \tag{6}$$

The essential part of the contribution made by the spin-orbit term comes from the $\vec{L}\cdot\vec{S}$ dependence. However, to make the effect to peak at the nuclear surface the radial part of the term can be taken to be

$$v_{\mathrm{LS}}(r) = v_{\mathrm{LS}}^0 \left(\frac{r_0}{\hbar}\right)^2 \frac{1}{r}\left[\frac{\mathrm{d}}{\mathrm{d}r}\frac{1}{1+e^{(r-R)/a}}\right] \tag{7}$$

with the spin-orbit interaction strength $v_{\mathrm{LS}}^0 = 0.44V_0$.

After specifying the single-particle Hamiltonian, the discrete nucleon single-particle states are now described by the eigenvectors of the Schödinger equation

$$h_{lj}|nljm\rangle = \epsilon_{nlj}|nljm\rangle. \tag{8}$$

The eigenvalue problem can be solved for example by expanding the non-trivial radial part of the solution in terms of radial harmonic oscillator wave functions [2]. The obtained single-particle energies ϵ_{nlj} are needed in the BCS calculations. It should be noted that single-particle states with discrete positive energies, the so-called quasi-stationary states, are a result of the 'centrifugal' $l(l+1)/r^2$ dependent term of the Schrödinger equation and the Coulomb potential [2].

1.2 BSC theory

The BCS quasiparticle creation and annihilation operators $a_\alpha^\dagger$ and a_α are defined via the Bogoliubov-Valantin transformation [2]

$$\begin{aligned} a_\alpha^\dagger &= u_a c_\alpha^\dagger + v_a \tilde{c}_\alpha \\ \tilde{a}_\alpha &= u_a \tilde{c}_\alpha - v_a c_\alpha^\dagger. \end{aligned} \tag{9}$$

Operators $c_\alpha^\dagger$ and c_α are the usual particle-creation and -annihilation operators. The index notation used here is the one introduced by Baranger. This means that $\alpha = \{a,\, m_\alpha\}$ with $a = \{n_a,\, l_a,\, j_a\}$. Numbers n, l, j and m are the usual quantum numbers of the individual mean-field single-particle states. Operators $\tilde{a}_\alpha = (-1)^{j_a+m_\alpha}a_{-\alpha}$ and $\tilde{c}_\alpha = (-1)^{j_a+m_\alpha}c_{-\alpha}$ are the time-reversed conpanions of the corresponding annihilation operators a_α and c_α with the notation $-\alpha = \{a,\, -\mathrm{m}_\alpha\}$.

The BCS ground state $|\mathrm{BCS}\rangle$ that acts as a vacuum for the BCS quasiparticles is defined with an ansatz [2]

$$|\mathrm{BCS}\rangle = \prod_{\alpha>0}(u_a - v_a c_\alpha^\dagger \tilde{c}_\alpha^\dagger)|\mathrm{CORE}\rangle. \tag{10}$$

The state $|\mathrm{CORE}\rangle$ represents the effective particle vacuum. This vacuum is the inert nuclear core of the reference nucleus. The proper BCS vacuum is then obtained as a result of a variational procedure, where the occupation amplitudes u_a and v_a serve as variational parameters to minimize the ground state energy [2]. Protons and neutrons are treated separately in the variational procedure.

It should be noted that the BCS ground state (10) lacks a good particle number [2]. To cope with this shortcoming, it is required as a variational constraint that the average particle number should correspond to the number of active valence nucleons of the reference nucleus.

The standard nuclear Hamiltonian (1) consists of one-particle and two-particle parts. It can be written in occupation-number representation as

$$H = \sum_\alpha \epsilon_\alpha c_\alpha^\dagger c_\alpha + \frac{1}{4}\sum_{\alpha\beta\gamma\delta} \bar{v}_{\alpha\beta\gamma\delta} c_\alpha^\dagger c_\beta^\dagger c_\delta c_\gamma, \tag{11}$$

where the antisymmetrized two-body-interaction matrix elements are defined as $\bar{v}_{\alpha\beta\gamma\delta} = \langle\alpha\beta|V|\gamma\delta\rangle - \langle\alpha\beta|V|\delta\gamma\rangle$ [1, 2]. For the calculations presented in this text, the two-body matrix elements are obtained from a realistic Bonn meson-exchange potential by the use of a so-called G-matrix method [3]. The G-matrix method is needed to account for the Pauli exclusion principle inside the nuclear matter.

In order to use the nuclear Hamiltonian in BCS theory and later in the QRPA and MQPM treatments, it has to be transformed into its quasiparticle representation using the Bogoliubov-Valantin transformation (9). In this representation the Hamiltonian attains the form

$$H = H_{00} + H_{11} + H_{20} + H_{02} + H_{22} + H_{31} + H_{13} + H_{40} + H_{04}, \tag{12}$$

where the indices m and n of each term H_{mn} denote the number of quasiparticle creation and annihilation operators, respectively, of the term in question [2]. BCS theory deals only with the terms H_{00}, H_{11}, H_{20} and H_{02} of the Hamiltonian. The rest of the terms constitute the quasiparticle residual interactions V_{RES} and are treated by means of the QRPA and the MQPM.

To help to state the variational problem one can define an auxiliary Hamiltonian $\mathcal{H} = H - \lambda\hat{n}$ with $\hat{n}$ as the particle number operator $\sum c_\alpha^\dagger c_\alpha$. The quantity λ is an unknown parameter serving as the Lagrange undetermined multiplier of the variational problem. It turns out that the variational procedure modifies the new Hamiltonian in a such a way that [2]

$$\mathcal{H} = \mathcal{H}_0 + \mathcal{H}_1 + V_{\mathrm{RES}}, \quad \mathcal{H}_1 = \sum_\beta E_b\, a_\beta^\dagger a_\beta. \tag{13}$$

In other words, the minimization of the ground-state energy occurs only when the two-quasiparticle terms of the Hamiltonian $\mathcal{H}$ vanish. What remains are the constant

term $\mathcal{H}_0$, the one-quasiparticle term $\mathcal{H}_1$ and the residual interactions $V_{\rm RES}$. The first two terms of the auxiliary Hamiltonian (13) describe a quasiparticle mean field of non-interacting BCS quasiparticles [2]. The quatities E_a are the energies of the one-quasiparticle states.

In the present work the Biedenharn–Rose phase convention of the angular part of the single-particle wave functions is used [2]. In this convention the BCS equations that arise from the variational procedure are written as [2]

$$u_a = \frac{1}{\sqrt{2}}\sqrt{1+\frac{\eta_a}{E_a}}, \quad v_a = \frac{1}{\sqrt{2}}\sqrt{1-\frac{\eta_a}{E_a}} \quad \text{(occupation amplitudes)}, \tag{14}$$

$$E_a = \sqrt{\eta_a^2+\Delta_a^2} \quad \text{(quasiparticle energy)} \tag{15}$$

and

$$2\hat{j}_a\Delta_a = -\sum_b \frac{\hat{j}_b\Delta_b}{\sqrt{\eta_b^2+\Delta_b^2}}\,\langle a\,a\,;\,0|V|b\,b\,;\,0\rangle \quad \text{(gap equation)}. \tag{16}$$

Here, and on many other occasions likewise, the hat factor is defined as $\hat{j}=\sqrt{2j+1}$. In addition to these equations also needed is the particle-number expectation value

$$\bar{n} = \langle {\rm BCS}|\hat{n}|{\rm BCS}\rangle = \sum_a \hat{j_a}^{\,2} v_a^2 = \frac{1}{2}\sum_a \hat{j_a}^{\,2}\left(1-\frac{\eta_a}{E_a}\right). \tag{17}$$

The short-hand notation used in the relations (14)–(17) is

$$\eta_b = \epsilon_b - \lambda - \mu_b, \tag{18}$$

where the quantity μ_b, called the self-energy, is written as

$$\mu_b = -\hat{j_b}^{\,-2}\sum_{aJ} v_a^2\hat{J}^2[\mathcal{N}_{ab}(J)]^{-2}\,\langle a\,b\,;\,J|V|a\,b\,;\,J\rangle. \tag{19}$$

Self-energy is releated to the renormalization of the single-particle energies ϵ_a. The undetermined multiplier λ that now appears in Eq. (18) is actually the chemical potential of the particle system. Solving of the above BCS equations requires an iterative method [2].

In actual BCS calculations the interaction matrix elements for protons and neutrons are scaled separately by constanst $g^{(p)}_{\rm pair}$ and $g^{(n)}_{\rm pair}$ [2]. The values of the constants are chosen so that the lowest quasiparticle energies agree with the experimental pairing gaps. These can be calculated from the three-point formulas [2]

$$\Delta_p({}^A_Z X_N) = \frac{1}{4}(-1)^{Z+1}\left[S_p(A+1,Z+1) - 2S_p(A,Z) + S_p(A-1,Z-1)\right] \tag{20}$$

and

$$\Delta_n({}^A_Z X_N) = \frac{1}{4}(-1)^{A-Z+1}\left[S_n(A+1,Z) - 2S_n(A,Z) + S_n(A-1,Z)\right]. \tag{21}$$

The quantities S_p and S_n are the needed experimental proton and neutron separation energies.

1.3 Quasiparticle random-phase approximation

After the BCS ground-state, along with a collection of several one-quasiparticle excited states, are defined, it is time to move on to the description of the two-quasiparticle excitations of the reference nucleus. In this work, this task is performed by using the quasiparticle random-phase approximation (QRPA) that takes into account the terms H_{22}, H_{40} and H_{04} of the residual interactions of the Hamiltonian (12) [1, 2].

The basic two-quasiparticle excitations of the QRPA theory, the so-called QRPA phonons, are created by an operator [1, 2]

$$Q^\dagger_\omega = \sum_{a\leq b} \left[X^\omega_{ab} A^\dagger_{ab}(JM) - Y^\omega_{ab} \tilde{A}_{ab}(JM) \right]. \tag{22}$$

According to the adopted notation, the index ω stands for the angular momentum J_ω, the parity π_ω and the additional quantum number k_ω that is used to make a distinction between different states with the same J_ω and π_ω. The operators $A^\dagger_{ab}$ and $\tilde{A}_{ab}$ that appear in (22) are the quasiparticle pair creation operator

$$A^\dagger_{ab}(JM) = \mathcal{N}_{ab}(J) \, [a^\dagger_a a^\dagger_b]_{JM} \tag{23}$$

and the time-reversed quasiparticle pair annihilation operator

$$\tilde{A}_{ab}(JM) = (-1)^{J+M} A_{ab}(J,-M) = -\mathcal{N}_{ab}(J) \, [\tilde{a}_a \tilde{a}_b]_{JM}. \tag{24}$$

The amplitudes X^ω and Y^ω related to the two-quasiparticle configuration mixing must be determined by solving the QRPA equations. These equations can be derived by using the equations-of-motion method introduced by Rowe [4]. Combining these equations together results in a matrix equation

$$\begin{bmatrix} A & B \\ -B^* & -A^* \end{bmatrix} \begin{bmatrix} X^\omega \\ Y^\omega \end{bmatrix} = E_\omega \begin{bmatrix} X^\omega \\ Y^\omega \end{bmatrix}, \tag{25}$$

where the submatrices A and B are defined with elements

$$A(ab,cd;J) = \langle \mathrm{BCS} | [A_{ab}(JM), \mathcal{H}, A^\dagger_{cd}(JM)] | \mathrm{BCS} \rangle \tag{26}$$

and

$$B(ab,cd;J) = -\langle \mathrm{BCS} | [A_{ab}(JM), \mathcal{H}, \tilde{A}_{cd}(JM)] | \mathrm{BCS} \rangle. \tag{27}$$

The mathematical operation inside (26) and (27) is the double commutator. For the Bose-like phonon excitations that are used here this is

$$[A,B,C] = \frac{1}{2} \left\{ \left[A, [B,C] \right] + \left[[A,B], C \right] \right\}. \tag{28}$$

The Hamiltonian that appears in these commutators is the auxiliary Hamiltonian (13). As indicated by the adopted notation, the submatrices A and B are both independent of the projection quantum number M [2].

The submatrix A is the same as in the quasiparticle Tamm–Dancoff approximation (QTDA) [2]. The contributions to it come from the quasiparticle mean field and the term H_{22}. The submatrix B is called the correlation matrix and from the definition

(27) it can be seen that only the four-quasiparticle term H_{40} contributes to it. The explicit expressions for the elements of the matrices A and B are [2]

$$\begin{aligned} A(ab,cd;J) = {} & (E_a+E_b)\delta_{ac}\delta_{bd} \\ & - 2\mathcal{N}_{ab}(J)\mathcal{N}_{cd}(J)\big[(u_a u_b u_c u_d + v_a v_b v_c v_d)G(ab,cd;J) \\ & + (u_a v_b u_c v_d + v_a u_b v_c u_d)F(ab,cd;J) \\ & - (-1)^{j_c+j_d+J}(u_a v_b v_c u_d + v_a u_b u_c v_d)F(ab,dc;J)\big] \end{aligned} \tag{29}$$

and

$$\begin{aligned} B(ab,cd;J) = {} & 2\mathcal{N}_{ab}(J)\mathcal{N}_{cd}(J)\big[(u_a u_b v_c v_d + v_a v_b u_c u_d)G(ab,cd;J) \\ & - (u_a v_b v_c u_d + v_a u_b u_c v_d)F(ab,cd;J) \\ & + (-1)^{j_c+j_d+J}(u_a v_b u_c v_d + v_a u_b v_c u_d)F(ab,dc;J)\big]. \end{aligned} \tag{30}$$

The above expressions are written in terms of the Baranger matrix elements [2]

$$G(ab,cd;J) = -\frac{1}{2}\big[\mathcal{N}_{ab}(J)\mathcal{N}_{cd}(J)\big]^{-1}\langle a\,b\,;J|V|\,c\,d\,;J\rangle \tag{31}$$

and

$$\begin{aligned} F(ab,cd;J) &= -\frac{1}{2}\langle a\,b^{-1}\,;J|V_{\rm RES}|\,c\,d^{-1};J\rangle \\ &= \frac{1}{2}\sum_{J'}\big[\mathcal{N}_{ad}(J')\mathcal{N}_{cb}(J')\big]^{-1}\hat{J'}^2\left\{\begin{array}{ccc} j_a & j_b & J \\ j_c & j_d & J' \end{array}\right\}\langle a\,d\,;J'|V|\,c\,b\,;J'\rangle. \end{aligned} \tag{32}$$

The two-body matrix elements of (31) and (32) are taken from the adopted Bonn meson-exchange potential. The notation a^{-1} in the particle-hole matrix element (32) is used to indicate the hole character of the orbital a. Here, the particle-hole matrix element is readily related to the used two-body matrix elements via the generalized Pandya transformation (32).

The introduction of the correlation matrix B means that the BCS ground-state $|\mathrm{BCS}\rangle$ is not actually the exact ground state for the QRPA excitations[2] [2]. However, the effect of the correlation matrix B is small and due to this the QRPA ground-state can be written schematically in the form

$$|\mathrm{QRPA}\rangle = |\mathrm{BCS}\rangle \;+\; \text{small corrections.} \tag{33}$$

The explicit form of the ground-state with its four-quasiparticle, eight-quasiparticle, etc. components can be found - but not needed in the treatment of this text - by using the Thouless theorem [2].

The structure of the QRPA matrix in the matrix equation (25) yields a non-hermitian eigenvalue problem. The solution can be obtained by using a method descriped in [2] which utilizes similarity transformations in the diagonalization of the QRPA matrix. As an effect of this non-hermiticity, the eigenvalue problem leads to both positive-energy and negative-energy solutions. In the QRPA formalism only the positive-energy solutions are accepted as physical solutions [2].

In actual QRPA calculations the interaction matrix elements are scaled by the constants $g_{\rm pp}$ and $g_{\rm ph}$ for each different J^π multipoles [2]. This is done to fit the multipoles to experimental energy levels of the chosen reference nucleus and thus to ensure a better agreement with experimental data.

---

2. In the case of QTDA theory the BCS ground-state $|\mathrm{BCS}\rangle$ is the exact ground state for the QTDA excitations.

1.4 Microscopic quasiparticle-phonon model

The final step is to take into account the terms H_{13} and H_{31} of the Hamiltonian (12). A fully microscopic way to do this is the microscopic quasiparticle-phonon model with its three-quasiparticle excitations [1].

The MQPM three-quasiparticle excitations are constructed by combining the BCS one-quasiparticle and the QRPA two-quasiparticle states. The operator that creates these excitations is written in a form [1]

$$\Gamma_i^\dagger(jm) = \sum_n C_n^i a_{njm}^\dagger + \sum_{a\omega} D_{a\omega}^i \left[a_a^\dagger Q_\omega^\dagger\right]_{jm}. \tag{34}$$

According to (34) each state is allowed to be built from both one-quasiparticle and one-quasiparticle-plus-phonon components. This is a drastic improvement over the simple one-quasiparticle description and offers a much richer spectrum of excited states of an odd-A nucleus.

Application of the equations-of-motion method of [4] to the excitations (34) leads to a generalized real symmetric eigenvalue problem [1]

$$\begin{bmatrix} A & B \\ B^T & A' \end{bmatrix} \begin{bmatrix} C^i \\ D^i \end{bmatrix} = \Omega_i \begin{bmatrix} 1 & 0 \\ 0 & N \end{bmatrix} \begin{bmatrix} C^i \\ D^i \end{bmatrix}. \tag{35}$$

The submatrices A and A' are the interaction matrices between two one-quasiparticle states and between two quasiparticle-phonon states, respectively. These matrices are defined with elements

$$A(a,a';j) = \langle \mathrm{BCS}|[a_a, H, a_{a'}^\dagger]|\mathrm{BCS}\rangle = E_a \delta_{aa'} \tag{36}$$

and

$$\begin{aligned} A'(\omega a,\omega' a';j) &= \langle \mathrm{BCS}|\,[\,[a_a^\dagger Q_\omega^\dagger]_j^\dagger, H, [a_{a'}^\dagger Q_{\omega'}^\dagger]_j\,]\,|\mathrm{BCS}\rangle \\ &= \frac{1}{2}(\hbar\Omega_\omega + E_a + \hbar\Omega_{\omega'} + E_{a'})N(\omega a,\omega' a';j) \\ &\quad - \frac{1}{2}\hat{J}_\omega \hat{J}_{\omega'} \sum_b \left\{ \begin{array}{ccc} j_{a'} & j_b & J_\omega \\ j_a & j & J_{\omega'} \end{array} \right\} (\hbar\Omega_\omega + E_a + \hbar\Omega_{\omega'} + E_{a'} - 2E_b) \\ &\quad \times \bar{X}_{ba'}^\omega \bar{X}_{ba}^{\omega'} \sigma_{ba}^{-1} \sigma_{ba'}^{-1} \\ &\quad + \frac{1}{2}\hat{J}_\omega \hat{J}_{\omega'} \sum_b \frac{\delta_{jj_b}}{\hat{j}^2} (-\hbar\Omega_\omega - E_a - \hbar\Omega_{\omega'} - E_{a'} - 2E_b) \bar{Y}_{ba}^\omega \bar{Y}_{ba'}^{\omega'} \sigma_{ba}^{-1} \sigma_{ba'}^{-1}, \end{aligned} \tag{37}$$

where the quantities $\hbar\Omega_\omega$ denote the QRPA phonon energies. The overlap matrix elements for two three-quasiparticle states are

$$N(\omega a,\omega' a';j) = \langle \mathrm{BCS}|\,[\,[a_a^\dagger Q_\omega^\dagger]_j^\dagger, [a_{a'}^\dagger Q_{\omega'}^\dagger]_j\,]\,|\mathrm{BCS}\rangle = \delta_{\omega\omega'}\delta_{aa'} + K(\omega a,\omega' a';j), \tag{38}$$

where the K matrix is defined as

$$K(\omega a,\omega' a';j) = \hat{J}_\omega \hat{J}_{\omega'} \sum_b \left[\left\{ \begin{array}{ccc} j_{a'} & j_b & J_\omega \\ j_a & j & J_{\omega'} \end{array} \right\} \bar{X}_{ba'}^\omega \bar{X}_{ba}^{\omega'} - \frac{\delta_{jj_b}}{\hat{j}^2} \bar{Y}_{ba}^\omega \bar{Y}_{ba'}^{\omega'} \right] \sigma_{ba}^{-1} \sigma_{ba'}^{-1}. \tag{39}$$

Here, the adopted notation is that $\sigma_{aa'} = \sqrt{1+\delta_{aa'}}$. The $\bar{X}$ amplitudes are symmetrized counterparts of the X amplitudes of (22) and are defined as $\bar{X}_{aa'}^\omega =$

$X^{\omega}_{aa'} - (-1)^{j_a+j_{a'}-J_\omega} X^{\omega}_{a'a}$, which holds likewise for the $\bar{Y}$ amplitudes. The interaction matrix elements between the one-quasiparticle and the quasiparticle-phonon states are defined as

$$\begin{aligned} B(\omega a, a'; j) &= \langle \mathrm{BCS} | \, [Q_\omega a_a]_j H a^\dagger_{a'} \, | \mathrm{BCS} \rangle \\ &= \frac{1}{3} \frac{\hat{J}_\omega}{\hat{j}_{a'}} \sum_{b \le b'} H_{pp}(bb'aa'J_\omega)(u_b u_{b'} X^{\omega}_{bb'} - v_b v_{b'} Y^{\omega}_{bb'}) \sigma^{-1}_{bb'} \\ &\quad - \frac{1}{3} \frac{\hat{J}_\omega}{\hat{j}_{a'}} \sum_{b \le b'} H_{hh}(bb'aa'J_\omega)(v_b v_{b'} X^{\omega}_{bb'} - u_b u_{b'} Y^{\omega}_{bb'}) \sigma^{-1}_{bb'} \\ &\quad + \frac{1}{3} \frac{\hat{J}_\omega}{\hat{j}_{a'}} \sum_{b \le b'} H_{ph}(bb'aa'J_\omega)(u_b v_{b'} X^{\omega}_{bb'} + v_b u_{b'} Y^{\omega}_{bb'}) \sigma^{-1}_{bb'} \\ &\quad - \frac{1}{3} \frac{\hat{J}_\omega}{\hat{j}_{a'}} \sum_{b \le b'} H_{hp}(bb'aa'J_\omega)(v_b u_{b'} X^{\omega}_{bb'} + u_b v_{b'} Y^{\omega}_{bb'}) \sigma^{-1}_{bb'}. \end{aligned} \tag{40}$$

The four different H factors included in (40) are

$$H_{pp}(bb'aa'J) = 2 v_b u_{b'} G(bb'aa'J) \tag{41}$$

$$H_{hh}(bb'aa'J) = 2 u_b v_{b'} G(bb'aa'J) \tag{42}$$

$$H_{ph}(bb'aa'J) = 2 v_b v_{b'} F(bb'aa'J) + 2 u_b u_{b'} F(b'baa'J)(-1)^{j_b+j_{b'}+J} \tag{43}$$

and

$$H_{hp}(bb'aa'J) = 2 u_b u_{b'} F(bb'aa'J) + 2 v_b v_{b'} F(b'baa'J)(-1)^{j_b+j_{b'}+J} \tag{44}$$

The quantities G and F are the Baranger matrix elements of (31) and (32).

Solving of the eigenvalue problem can be done using a method described in [1]. This involves diagonalizing the submatrix N and forming a complete set of basis states by removing the ones with zero eigenvalue. In practice the calculation accounts only for the lowest-energy phonons that dominate in the low-energy region of the odd-A nucleus level scheme.

When a nuclear model is adopted, one can calulate the reduced CCTD matrix elements for β^- transitions (see Chapter 2 for the discussion on β^- transitions). According to [5] the needed elements in the MQPM formalism are

$$(p||[\, c^\dagger_{p'} \tilde{c}_{n'}\,]_L||n) = \hat{L} u_p u_n \delta_{pp'} \delta_{nn'} \tag{45}$$

and

$$(n||[\, c^\dagger_{p'} \tilde{c}_{n'}\,]_L||p) = \hat{L} v_n v_p \delta_{nn'} \delta_{pp'} (-1)^{j_{n'}+j_{p'}+L} \tag{46}$$

for transitions between one-quasiparticle states (between particle states and between hole states, respectively) and

$$\begin{aligned} (\omega p j||[\, c^\dagger_{p'} \tilde{c}_{n'}\,]_L||n) = (-1)^{j_p+J_\omega-j} \hat{J}_\omega \hat{L} \hat{j} \Bigg[& \begin{Bmatrix} j_n & j & L \\ j_p & j_{n'} & J_\omega \end{Bmatrix} \\ & \times \bar{X}^{\omega}_{nn'} u_{p'} v_{n'} \sigma^{-1}_{nn'} \delta_{pp'} (-1)^{j_n+j+L} + \frac{\delta_{jj_{p'}}}{\hat{j}^2} \bar{Y}^{\omega}_{pp'} v_{p'} u_{n'} \sigma^{-1}_{pp'} \delta_{nn'} \Bigg] \end{aligned} \tag{47}$$

and

$$(\omega nj||[\,c^{\dagger}_{p'}\tilde{c}_{n'}\,]_L||p) = -(-1)^{j_{p'}+j_{n'}+L}(-1)^{j_n+J_\omega-j}\hat{J}_\omega\hat{L}\hat{j}\left[\begin{Bmatrix} j_p & j & L \\ j_n & j_{p'} & J_\omega \end{Bmatrix}\right.$$
$$\left.\times\,\bar{X}^{\omega}_{pp'}v_{n'}u_{p'}\sigma^{-1}_{pp'}\delta_{nn'}(-1)^{j_p+j+L} + \frac{\delta_{jj_{n'}}}{\hat{j}^2}\bar{Y}^{\omega}_{nn'}u_{n'}v_{p'}\sigma^{-1}_{nn'}\delta_{pp'}\right] \tag{48}$$

for the transitions between one-quasiparticle and quasiparticle-phonon states. The auxiliary quantities $\bar{X}^{\omega}_{aa'}$, $\bar{Y}^{\omega}_{aa'}$ and $\sigma_{aa'}$ are defined in same way as in (37), (38) and (39). Furthermore, for transitions between two quasiparticle-phonon states one needs

$$\begin{aligned}(\omega nj||[\,c^{\dagger}_{p'}\tilde{c}_{n'}\,]_L||\omega' pj') = -\Bigg[&(-1)^{j_p+J_\omega-j}\begin{Bmatrix} j & L & j' \\ j_{n'} & J_\omega & j_{p'} \end{Bmatrix}\delta_{pp'} \\ &\times\left(\frac{1}{2}\delta_{nn'}\delta_{\omega\omega'} + K(\omega n',\omega' n;j')\right) + (-1)^{j_{p'}+J_{\omega'}-j}\begin{Bmatrix} j & L & j' \\ j_{n'} & J_{\omega'} & j_{p'} \end{Bmatrix}\delta_{nn'} \\ &\times\left(\frac{1}{2}\delta_{pp'}\delta_{\omega\omega'} + K(\omega p,\omega' p';j)\right)\Bigg]\hat{j}\hat{L}\hat{j}'(-1)^{j+L+j'}v_{p'}v_{n'} \\ &-\left[\begin{Bmatrix} j & L & j' \\ j_p & j_{p'} & J_{\omega'} \end{Bmatrix}\bar{X}^{\omega'}_{p'p}\bar{X}^{\omega}_{nn'}(-1)^{j_{n'}+j_{p'}-L} + \frac{\delta_{jj_{n'}}\delta_{j'j_{p'}}}{\hat{j}^2\hat{j}'^2}\bar{Y}^{\omega}_{pp'}\bar{Y}^{\omega'}_{n'n}\right] \\ &\times\sigma^{-1}_{nn'}\sigma^{-1}_{pp'}\hat{j}\hat{L}\hat{j}'(-1)^{j_p+J_\omega-j}\hat{J}_\omega\hat{J}_{\omega'}u_{p'}u_{n'}\end{aligned} \tag{49}$$

from which the other matrix element $(\omega pj||[\,c^{\dagger}_{p'}\tilde{c_{n'}}\,]_L||\omega' nj')$ can be obtained by substituting $u_a \to v_a$ and $v_a \to -u_a$ [5]. The quantities $K(\omega a,\omega' a';j)$ are taken from the relation (39).

2 Nuclear beta minus decay

The discussion on the nuclear β^- decay begins in this section with an overview to the deeper, particle level properties of the process. This introduction is then followed by a streamlined discussion on the general theory of forbidden β^- transitions. Also the drastically simplified theory for allowed transitions is presented at the end of the chapter.

All the actual relations presented in the section 2.2 are taken from the articles [5] and [6]. A much more comprehensive discussion on the theory of beta decay can be found in [7], on which the treatments in the articles [5] and [6] are based.

2.1 General properties of beta minus transitions

The nuclear β^- decay, expressed as

$$ {}^{A}_{Z}X_N \rightarrow {}^{A}_{Z+1}X_{N-1} + e^- + \bar{\nu}_e \,, $$

is a process where one of the neutrons within the decaying neutron-rich mother nucleus is converted into a proton. This conversion is accompanied by an emission of an electron and an electron antineutrino. As the increase of the proton number Z by one unit results in a decrease of the neutron number N by one unit, the process involves only isobars of the same mass number A. Using atomic masses, the Q-value of the decay is expressed as

$$ Q = [\, m({}^{A}_{Z}X_N) - m({}^{A}_{Z+1}X_{N-1}) \,]c^2 + E^*_i - E^*_f, \tag{50} $$

were the quantities E^*_i and E^*_f are the excitation energies of the intial and final state nuclides ${}^{A}_{Z}X_N$ and ${}^{A}_{Z+1}X_{N-1}$, respectively [8].

The conversion of an uncharged nucleon to a charged one is a weak-interaction process depicted by a Feynman diagram of Figure 1a. The weak charge-changing interaction is mediated by the negatively charged vector boson W^-. However, due to the large 80 GeV/c^2 mass of W^- and the modest energy range of nuclear beta decay, the process can be described as a pointlike interaction with an effective Fermi decay strength constant G_F (see Figure 1b) [9]. This pointlike interaction process has an invariant amplitude of the form

$$ \mathfrak{M}(n \rightarrow pe^-\bar{v}_e) = \frac{4G_F}{\sqrt{2}} \left[\frac{1}{2}\bar{u}_p\gamma_\mu(1 - (\tfrac{g_A}{g_V})\gamma_5)u_n \right] \left[\frac{1}{2}\bar{u}_e\gamma^\mu(1-\gamma^5)u_{\bar{\nu}_e} \right]. \tag{51} $$

The quantities inside the square brakets of (51) are the charge-raising hadronic current and the charge-lowering leptonic current, respectively. The mixture $\gamma^\mu - \gamma^\mu\gamma^5$ of the γ-matices yields a V-A (vector-minus-axial-vector) structure that leads to the observed parity non-conserving nature of weak interactions [9].

For the leptonic current this V-A structure is exactly the correct one. For the hadronic current however a renormalized combination $\mathrm{V} - (\frac{g_A}{g_V})\mathrm{A}$ is more appropriate due to the effects of color forces between the quarks [9]. The values

$$ g_V = 1 \,, \quad g_A = 1.25 \tag{52} $$

of the vector coupling constant g_V and axial-vector coupling constant g_A are determined by the CVC (conserved vector current) hypotesis and the PCAC (partially

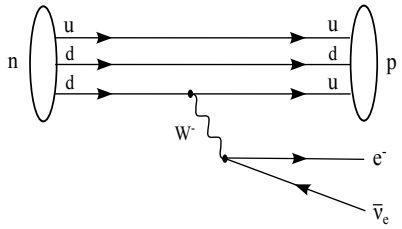

(a) The decay of a free neutron on quark level. Vector boson W^- mediates the weak interaction.

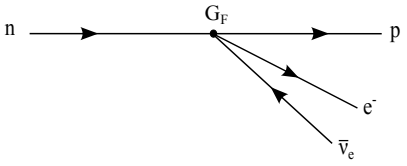

(b) The decay of a free neutron depicted as a point-like interaction process with an effective Fermi decay strength constant G_F.

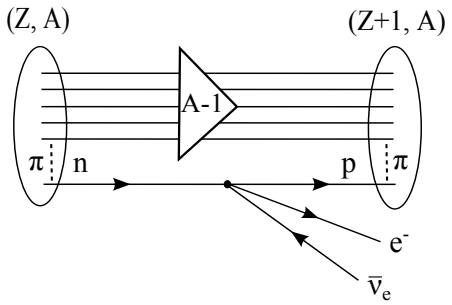

(c) The nuclear β^- decay when the impulse approximation is applied to the decaying neutron. During the decay process the remaining $A-1$ nucleons act only as spectators.

Figure 1: Feynman diagrams depicting the weak-interaction process that leads to the conversion of a neutron into a proton.

conserved axial-vector current) hypotesis, of the standard model of electroweak interactions [2].

In nuclear β decay the decay process of Figure 1b happens in a nuclear enviroment. This means that in addition to the weak interaction, also present is the strong nuclear force between the nucleons. To deal with the complications resulting from this strong interaction, a treatment called the impulse approximation is used [2, 5]. In this approximative scheme the decaying nucleon feels only the weak interaction at the moment of its decay. The remaining $A-1$ nucleons act as spectators. This simplified reaction mechanism is depicted in Figure 1c.

2.2 General theory of forbidden beta minus transitions

In the K-forbidden ($K = 1, 2, 3, ...$) β^- transition the final state leptons leave the nucleus with non-zero orbital angular momenta with respect to it. This causes the angular momentum of the nuclear state to change from an initial value J_i to some final value J_f according to the selection rules of Table 1 [2]. Depending on the forbiddenness of the transition, the angular momentum change can also be accompanied by a change of parity of the nuclear state wave function.

Table 1: Angular momentum and parity selection rules for forbidden transitions. Quantity K represents the degree of forbiddenness of the transition.

K	$\Delta J = \lvert J_f - J_i \rvert$	$\pi_f \pi_i$
1	0, 1, 2	-1
2	2, 3	+1
3	3, 4	-1
4	4, 5	+1

The probability for the emitted electron to have its total energy in a small interval from W_e to $W_e + \mathrm{d}W_e$ is [5]

$$P(W_e)\mathrm{d}W_e = \frac{G_F^2}{(\hbar c)^6}\frac{1}{2\pi^3\hbar}C(W_e)p_e c W_e (W_0 - W_e)^2 F_0(Z, W_e)\mathrm{d}W_e. \tag{53}$$

Here, W_0 is the end-point energy of the beta spectrum. The quantity p_e is the momentum of the electron and Z the proton number of the daughter nucleus. Fermi function $F_0(Z, W_e)$ takes into account the Coulumbic interaction between the emitted electron and the nucleus. $C(W_e)$ is the shape factor and $p_e c W_e (W_0 - W_e)^2$ a kinematic factor that arises from the available phase space of the final-state leptons.

Due to the electron's negative charge the Coulombic interaction between the electron and the nucleus is attractive. Qualitatively, this has an effect of slightly shifting the energy spectrum of the emitted electron to lower energies compared to a case, where the electron would have no electric charge at all [8]. For positively charged positron that is emitted in β^+ decay the effect is just the opposite.

Intergration of Eq. (53) over the possible electron energy range allowes one to write the partial half-life of the transition now in a form $t_{1/2} = \kappa/\tilde{C}$ [5], where the constant κ is given by

$$\kappa = \frac{2\pi^3\hbar\,\ln 2}{(m_e c^2)^5 G_F^2/(\hbar c)^6} \approx 6147\,\mathrm{s} \tag{54}$$

and the quantity $\tilde{C}$ is the integrated shape factor

$$\tilde{C} = \int_1^{w_0} C(w_e) p w_e (w_0 - w_e)^2 F_0(Z, w_e) dw_e. \tag{55}$$

The expression (55) is made unitless by scaling the quantities W_0, W_e and p_e with the rest-mass energy of the electron. In other words $w_0 = W_0/(m_e c^2)$, $w_e = W_e/(m_e c^2)$ and $p = p_e/(m_e c^2)$.

Excluding at first the case with angular momentum change $\Delta J = |J_f - J_i| = 0$, it is possible to write the shape factor C in a form [5]

$$\begin{aligned} C(w_e) = \left(\frac{m_e c^2}{\hbar c}\right)^{2K} \Bigg[& \sum_{k_e + k_\nu = K+1} \lambda_{k_e} (w_e^2 - 1)^{k_e - 1} (w_0 - w_e)^{2(k_\nu - 1)} g_V^2 D^2_{K k_e k_\nu} \tilde{\mathcal{A}}_K \\ & + \sum_{k_e + k_\nu = K+2} \lambda_{k_e} (w_e^2 - 1)^{k_e - 1} (w_0 - w_e)^{2(k_\nu - 1)} g_V^2 \tilde{D}^2_{K k_e k_\nu} \mathcal{B}_K \Bigg] \end{aligned} \tag{56}$$

The positive integers k that appear in this expression result from the expansion of the final-state lepton wave functions into partial waves. These numbers are related to the orbital (l) and total (j) angular momentum of the leptons according to relation

$$k = \begin{cases} l, & \text{for } j = l - \frac{1}{2} \\ l+1, & \text{for } j = l + \frac{1}{2} \end{cases} . \tag{57}$$

The two summations in (56) are understood so that the leading contributions to them come from the lowest-order terms of the expansions that satisfy the relations $k_e + k_\nu = K + 1$ and $k_e + k_\nu = K + 2$.

The quantity λ_{k_e} that appears in (56) is

$$\lambda_{k_e} = \frac{F_{k_e-1}(Z, w_e)}{F_0(Z, w_e)}, \tag{58}$$

where $F_{k_e-1}(Z, w_e)$ is the generalized Fermi function

$$\begin{aligned} F_{k_e-1}(Z, w_e) = & 4^{k_e-1}(2k_e)(k_e + \gamma_{k_e})[(2k_e - 1)!!]^2 \\ & \times e^{\pi y} \left(\frac{2p_e R}{\hbar}\right)^{2(\gamma_{k_e} - k_e)} \left(\frac{|\Gamma(\gamma_{k_e} + iy)|}{\Gamma(1 + 2\gamma_{k_e})}\right)^2 . \end{aligned} \tag{59}$$

The two dimensionless quantities inside the Fermi function are $y = (\alpha Z w_e)/(p_e c)$ and $\gamma_{k_e} = \sqrt{k_e^2 - (\alpha Z)^2}$. The quantity α is the fine structure constant and Γ the usual gamma function. Furthermore,

$$D_{K k_e k_\nu} = \frac{1}{\sqrt{2}} \sqrt{\frac{(2K)!!}{(2K+1)!!}} \frac{1}{\sqrt{(2k_e - 1)!(2k_\nu - 1)!}} \tag{60}$$

and

$$\tilde{D}_{K k_e k_\nu} = \sqrt{\frac{(2K)!!}{(2K+1)!!}} \frac{1}{\sqrt{(2k_e - 1)!(2k_\nu - 1)!}}. \tag{61}$$

The explicit expressions for the quantities $\tilde{\mathcal{A}}_K$ and $\mathcal{B}_K$ involve both kinematical factors and nuclear form factors [5]. The nuclear form factors carry all the nuclear structure information. In the impulse approximation the form factors can be stated in terms of six nuclear matrix elements, namely M_1, M_2, M_3, M_4, $M_2^{(k_e)}$ and $M_3^{(k_e)}$ [5]. Adopting the notations

$$M_\pm = M_2 \pm \sqrt{\frac{K+1}{K}} \frac{g_A}{g_V} M_3 \tag{62}$$

and

$$M_-^{(k_e)} = M_2^{(k_e)} - \sqrt{\frac{K+1}{K}} \frac{g_A}{g_V} M_3^{(k_e)} \tag{63}$$

the expressions for $\tilde{\mathcal{A}}_K$ and $\mathcal{B}_K$ become

$$\begin{aligned}
\tilde{\mathcal{A}}_K =& \frac{2K+1}{K}\tilde{M}_1^2 + \frac{1}{(2k_\nu+1)^2}(w_0-w_e)^2 M_+^2 \\
&+ \frac{1}{(2k_e+1)^2}\left[(\tilde{\alpha}Z)^2(M_-^{(k_e)})^2 + 2(\tilde{\alpha}Z)w_e M_- M_-^{(k_e)} + (1+w_e^2)M_-^2\right] \\
&- \frac{2\gamma_{k_e}}{k_e w_e(2k_e+1)^2}\left[(\tilde{\alpha}Z)M_- M_-^{(k_e)} + w_e M_-^2\right] \\
&- \frac{2}{2k_e+1}\sqrt{\frac{2K+1}{K}}\left[(\tilde{\alpha}Z)\tilde{M}_1 M_-^{(k_e)} + w_e \tilde{M}_1 M_-\right] \\
&+ \frac{2}{2k_e+1}\sqrt{\frac{2K+1}{K}}\frac{\gamma_{k_e}}{k_e w_e}\tilde{M}_1 M_- - \frac{2}{2k_\nu+1}\sqrt{\frac{2K+1}{K}}(w_0-w_e)\tilde{M}_1 M_+ \\
&+ \frac{2}{(2k_e+1)(2k_\nu+1)}(w_0-w_e)\left[(\tilde{\alpha}Z)M_-^{(k_e)} + w_e M_-\right] M_+ \\
&- \frac{2}{(2k_e+1)(2k_\nu+1)}\frac{\gamma_{k_e}}{k_e w_e}(w_0-w_e) M_- M_+
\end{aligned} \tag{64}$$

and

$$\begin{aligned}
\mathcal{B}_K =& \frac{K+1}{(2k_e-1)(2k_\nu-1)}\left[M_2^2 + 2\frac{g_A}{g_V}\frac{k_e-k_\nu}{\sqrt{K(K+1)}}M_2 M_3\right. \\
&\left. + \left(\frac{g_A}{g_V}\right)^2 \frac{(k_e-k_\nu)^2}{K(K+1)}M_3^2\right] + \left(\frac{g_A}{g_V}\right)^2 M_4^2.
\end{aligned} \tag{65}$$

The new, scaled fine structure constant $\tilde{\alpha}$ that appears in these two expressions is defined as $\tilde{\alpha} = (\alpha\hbar)/(Rm_e c)$.

The nuclear matrix elements M_1–M_4 that arise from the impulse approximation can be written as

$$\tilde{M}_1 = \frac{\hbar c}{m_e c^2}M_1 = \frac{\hbar c}{m_e c^2}\frac{1}{\hat{J}_i}\sum_{pn}{}^V m_{K,K-1,1}(pn)(\psi_f||[\,c_p^\dagger \tilde{c}_n\,]_K||\psi_i), \tag{66}$$

$$M_2 = \frac{1}{\hat{J}_i}\sum_{pn}{}^V m_{KK0}(pn)(\psi_f||[\,c_p^\dagger \tilde{c}_n\,]_K||\psi_i), \tag{67}$$

$$M_3 = \frac{1}{\hat{J}_i}\sum_{pn}{}^A m_{KK1}(pn)(\psi_f||[\,c_p^\dagger \tilde{c}_n\,]_K||\psi_i) \tag{68}$$

and

$$M_4 = \frac{1}{\hat{J}_i}\sum_{pn}{}^A m_{K+1,K1}(pn)(\psi_f||[\,c_p^\dagger \tilde{c}_n\,]_{K+1}||\psi_i). \tag{69}$$

with p and n the proton and neutron indices, respectively. The charge-changing transition densities (CCTDs) $(\psi_f||[\,c_p^\dagger \tilde{c}_n\,]_K||\psi_i)$ dependent on the nuclear structure and in order to calculate these quantities an actual nuclear model must be specified. For the purposes of this text the chosen model is the MQPM discussed in Chap. 1. The explicit expressions for the relevant CCTD matrix elements were provided at the end of that chapter.

The reduced single-particle matrix elements ${}^{V/A}m_{KLS}(pn)$ of the expressions (66)–(69) are on the other hand completely independent of the nuclear model. Stated

explicitly, the elements are

$$
\begin{aligned}
{}^{V}m_{KK0}(pn) = & \, i^{\,l_p+l_n+K}(-1)^{j_p+j_n+1}\frac{1+(-1)^{l_p+l_n+K}}{2}\frac{\hat{j}_p\hat{j}_n}{\hat{K}}(j_p\,\tfrac{1}{2}\,j_n\,-\tfrac{1}{2}|K\,0) \\
& \times\Big[(-1)^{l_n+j_n-1/2}\langle r^K\rangle_{pn}\,\Delta(l_p l_n K) \\
& \quad +(-1)^{l_p+j_p-1/2}\left\{r^K\right\}_{\tilde{p}\tilde{n}}\,\Delta(\tilde{l}_p\tilde{l}_n K)\Big],
\end{aligned}
\tag{70}
$$

$$
\begin{aligned}
{}^{A}m_{KL1}(pn) = & \, i^{\,l_p+l_n+L}(-1)^{K+1}\frac{1+(-1)^{l_p+l_n+L}}{2}\frac{\hat{L}\hat{j}_p\hat{j}_n}{\hat{K}}(j_p\,\tfrac{1}{2}\,j_n\,-\tfrac{1}{2}|K\,0) \\
& \times\Big\{\left[\mathcal{A}_{KL}(pn)+\mathcal{B}_{KL}(pn)\right]\langle r^L\rangle_{pn}\Delta(l_p l_n L) \\
& \quad +(-1)^{l_p+l_n+j_p+j_n}\left[\mathcal{A}_{KL}(pn)-\mathcal{B}_{KL}(pn)\right]\left\{r^L\right\}_{\tilde{p}\tilde{n}}\Delta(\tilde{l}_p\tilde{l}_n L)\Big\}
\end{aligned}
\tag{71}
$$

and

$$
\begin{aligned}
{}^{V}m_{KL1}(pn) = & \, i^{\,l_p+l_n+L+1}\frac{1+(-1)^{l_p+l_n+L+1}}{2}\frac{\hat{L}\hat{j}_p\hat{j}_n}{\hat{K}}(j_p\,\tfrac{1}{2}\,j_n\,-\tfrac{1}{2}|K\,0) \\
& \times\Big\{(-1)^{K+l_n+j_n+1/2}\left[\mathcal{A}_{KL}(pn)+\mathcal{B}_{KL}(pn)\right]\left\{r^L\right\}_{p\tilde{n}}\Delta(l_p\tilde{l}_n L) \\
& \quad +(-1)^{K+l_p+j_p+1/2}\left[\mathcal{A}_{KL}(pn)-\mathcal{B}_{KL}(pn)\right]\left\{r^L\right\}_{\tilde{p}n}\Delta(\tilde{l}_p l_n K)\Big\}.
\end{aligned}
\tag{72}
$$

The notation $\Delta(l_1 l_2 L)$ accounts for the triangular conditions $|l_1 - l_2| \leq L \leq l_1 + l_2$ for the coupling of the angular momenta l_1, l_2 and L. If the triangular condition is satisfied the term affected by this coupling is left untouched. Otherwise the term must vanish. The quantity $\tilde{l}$ is an auxiliary quantum number defined as

$$
\tilde{l} = \begin{cases} l+1, & j = l+\frac{1}{2} \\ l-1, & j = l-\frac{1}{2} \end{cases} . \tag{73}
$$

The notation $\tilde{p}$ denotes a set of proton quantum numbers $\{n_p, \tilde{l}_p, j_p\}$. The same applies also to the auxiliary neutron index $\tilde{n}$ with the neutron quantum numbers.

The geometric factors $\mathcal{A}_{KL}(pn)$ and $\mathcal{B}_{KL}(pn)$ that appear inside the single-particle elements (70)–(72) are

$$
\mathcal{A}_{KL}(pn) = \frac{\hat{j}_p^2 + (-1)^{j_p+j_n+K}\hat{j}_n^2}{\sqrt{2K(K+1)(2L+1)}}(-1)^{K+1}(K\,1\,1\,-1|L\,0)(1-\delta_{K0}) \tag{74}
$$

and

$$
\mathcal{B}_{KL}(pn) = (-1)^{l_p+j_p-1/2+K}\frac{1}{\hat{L}}(K\,0\,1\,0|L\,0). \tag{75}
$$

The same single-particle elements also include radial factors

$$
\left\{r^L\right\}_{p\tilde{n}} = k(b)\left(b^{-1}\langle r^{L+1}\rangle_{pn} - 2\sqrt{n_n+j_n+1}\langle r^L\rangle_{p\tilde{n}}\right), \tag{76}
$$

$$
\left\{r^L\right\}_{\tilde{p}n} = k(b)\left(b^{-1}\langle r^{L+1}\rangle_{pn} - 2\sqrt{n_p+j_p+1}\langle r^L\rangle_{\tilde{p}n}\right) \tag{77}
$$

and

$$
\begin{aligned}
\left\{r^L\right\}_{\tilde{p}\tilde{n}} = & \, k(b)\Big(b^{-2}\langle r^{L+2}\rangle_{pn} - 2b^{-1}\sqrt{n_p+j_p+1}\langle r^{L+1}\rangle_{\tilde{p}n} \\
& - 2b^{-1}\sqrt{n_n+j_n+1}\langle r^{L+1}\rangle_{p\tilde{n}} \\
& + 4\sqrt{(n_n+j_n+1)(n_p+j_p+1)}\langle r^L\rangle_{\tilde{p}\tilde{n}}\Big).
\end{aligned}
\tag{78}
$$

The basic radial integral of the above factors is defined as

$$\langle r^L \rangle_{pn} = \int_0^\infty g_{n_p l_p}(r) r^L g_{n_n l_n} r^2 \mathrm{d}r, \tag{79}$$

where the function $g_{nl}(r)$ is the usual radial harmonic oscillator wave function. The prefactor $k(b)$ is defined as

$$k(b) = \frac{1}{2m_N b} = \frac{0.1051}{b\,[\mathrm{fm}]} \tag{80}$$

with b taken to be the harmonic oscillator parameter

$$b = \frac{197.33}{\sqrt{939\hbar\omega}}\,\mathrm{fm}, \qquad \hbar\omega = 45A^{-1/3} - 25A^{-2/3}. \tag{81}$$

Expressing the basic radial integrals as $(\mathrm{fm})^L$ allowes one to state all the single-particle matrix elements in units of $(\mathrm{fm})^L$.

The two remaining matrix elements $M_2^{(k_e)}$ and $M_3^{(k_e)}$ are just the same as M_2 and M_3, respectively, except for the Coulomb factor

$$I(k_e,1,1,1;r) = \begin{cases} \frac{3}{2} - \frac{2k_e+1}{2(2k_e+3)}\left(\frac{r}{R}\right)^2, & 0 \le r \le R \\ \frac{2k_e+1}{2k_e}\frac{R}{r} - \frac{3}{2k_e(2k_e+3)}\left(\frac{R}{r}\right)^{2k_e+1}, & r > R \end{cases} \tag{82}$$

that must be included inside the basic radial integrals (79) [5].

A drastic simplification occurs in the case of unique transitions where the change of angular momentum is maximal to the degree of forbiddenness of the transition, i.e. follows the relation $\Delta J = K + 1$. For these transitions only the element M_4 contributes to the decay half-life.

An important exception to general theory discussed above is the case of first forbidden transitions ($K = 1$), where it is possible to have $\Delta J = 0$, i.e. a zero change of angular momentum. In the case of β^- decay an extra term

$$\begin{aligned} C^{(1)} = \left(\frac{m_e c^2}{\hbar c}\right)^2 \Bigg[& g_A^2\Big(\tilde{M}_5 + \frac{w_0}{3}M_6 + \frac{\tilde{\alpha}Z}{3}M_6^{(1)}\Big)^2 + g_A^2\left(\frac{M_6}{3}\right)^2 \\ & - g_A^2\frac{2\gamma_1}{w_e}\Big(\tilde{M}_5 + \frac{w_0}{3}M_6 + \frac{\tilde{\alpha}Z}{3}M_6^{(1)}\Big)\frac{M_6}{3}\Bigg] \end{aligned} \tag{83}$$

must be added to the shape factor (56) [6]. The extra matrix elements thus needed to calculate the decay half-life are

$$\tilde{M}_5 = \frac{\hbar c}{m_e c^2}M_5 = \frac{\hbar c}{m_e c^2}\frac{1}{\hat{J}_i}\sum_{pn} {}^{AR}m_{00}(pn)(\psi_f||[\,c_p^\dagger \tilde{c_n}\,]_0||\psi_i) \tag{84}$$

and

$$M_6 = \frac{1}{\hat{J}_i}\sum_{pn} {}^{A}m_{001}(pn)(\psi_f||[\,c_p^\dagger \tilde{c_n}\,]_0||\psi_i). \tag{85}$$

The single-particle matrix element of (84) is written as

$$\begin{aligned} {}^{AR}m_{0L}(pn) = & \, i^{\,l_p+l_n+L+1}(-1)^{j_p+j_n}\frac{1+(-1)^{l_p+l_n+L+1}}{2}\frac{\hat{j_p}\hat{j_n}}{\hat{L}}(j_p\,\tfrac{1}{2}\,j_n\,-\tfrac{1}{2}|L\,0) \\ & \times\Big[\left\{r^L\right\}_{p\tilde{n}}\,\Delta(l_p\tilde{l}_n L) + (-1)^{j_p+j_n+L+1}\left\{r^L\right\}_{\tilde{p}n}\,\Delta(\tilde{l}_p l_n L)\Big]. \end{aligned} \tag{86}$$

The other one can be taken from (71) with $K = 0$ and $L = 0$. Again, the matrix element $M_6^{(1)}$ is just the same as M_6 except for the Coulomb factor (82) included inside the basic radial integrals.

2.3 Allowed beta minus transitions

The many complications of the general theory of forbidden beta transitions arise from the fact that the leptons leave the nucleus with non-zero angular momentum. When the leptons leave the nucleus with no orbital angular momentum with respect to it, the observed change ΔJ is completely caused by the intrinsic spin angular momenta of these leptons. Adding them up amounts a total of 0 or 1 with no change of parity.

The distinctive property of the allowed β transition theory is that the lepton kinematics are completely separated from the content carrying the nuclear structure information. The partial half-life can be written as

$$t_{1/2} = \frac{\kappa}{f_0(B_F + B_{GT})}, \tag{87}$$

where the constant κ is the same as in (54) [2]. The quantities B_F and B_{GT} are the Fermi and Gamow–Teller reduced transition probabilities

$$B_F = \frac{g_V^2}{2J_i + 1}|M_F|^2 \tag{88}$$

and

$$B_{GT} = \frac{g_A^2}{2J_i + 1}|M_{GT}|^2. \tag{89}$$

The Fermi and Gamow–Teller matrix elements M_F and M_{GT} of these quantities are written in a familiar manner:

$$M_F = \delta_{J_i J_f} \sum_{pn} m_F(pn)(\psi_f|||[\, c_p^\dagger \tilde{c_n}\,]_0||\psi_i) \tag{90}$$

and

$$M_{GT} = \sum_{pn} m_{GT}(pn)(\psi_f|||[\, c_p^\dagger \tilde{c_n}\,]_1||\psi_i), \tag{91}$$

where the reduced single-particle matrix elements are

$$m_F(pn) = \delta_{n_p n_n}\delta_{l_p l_n}\delta_{j_p j_n}\hat{j}_p \tag{92}$$

and

$$m_{GT}(pn) = \sqrt{2}\,\delta_{n_p n_n}\delta_{l_p l_n}\,\hat{j}_p\hat{j}_n(-1)^{l_p+j_p+3/2}\begin{Bmatrix} \frac{1}{2} & \frac{1}{2} & 1 \\ j_n & j_p & l_p \end{Bmatrix}. \tag{93}$$

The CCTDs of the matrix elements (90) and (91) are again obtained from the MQPM. The angular momentum selection rules that distinguish Fermi and Gamow–Teller type transitions from one another are given in Table 2 [2].

The part f_0 in the partial half-life expression (87) is a dimensioless phase-space factor for the final-state leptons. For β^- transitions it is written as

$$f_0 = \int_1^{w_0} F_0(Z, w_e)pw_e(w_0 - w_e)^2 dw_e. \tag{94}$$

The quantities that appear inside (94) are just the same ones as in the integrated shape factor (56).

Table 2: Angular momentum selection rules for Fermi and Gamow–Teller transitions. There is no parity change involved for any allowed transitions.

Type	$\Delta J = \lvert J_f - j_i \rvert$	$\pi_f \pi_i$
Fermi	0	+1
Gamow–Teller	1 ($J_i = 0$ or $J_f = 0$)	+1
Gamow–Teller	0, 1 ($J_i > 0$ and $J_f > 0$)	+1

3 Applications to the beta decay of Cd-115

In this chapter the theoretical framework is put into a test. In order to study the β^- decay of ^{115}Cd one must begin with the calculation of the needed CCTDs. Once these quantities are obtained they can be used to determine theoretical predictions for the partial half-lives of the different β^- transitions. These predictions can then be compared with experimentally confirmed results.

The reference nucleus for the MQPM calculations presented in this chapter is the even-even nucleus ^{114}Cd. The experimentally measured excitation level scheme of this nucleus as well as those of the mother and daughter nuclei ^{115}Cd and ^{115}In can be found from [10]. Also taken from [10] is the β decay scheme of ^{115}Cd that holds all the necessary information needed to calculate the experimental decay half-lives.

3.1 Beta decay calculations

The adopted valence space for the reference nucleus ^{114}Cd consists of proton single-particle orbitals 0f, 1p, 0g, 1d, 2s and $0h_{11/2}$ and neutron single-particle orbitals 1p, 0g, 1d, 2s, 0h, 1f, 2p and $0i_{13/2}$. This gives a total of $Z_{\text{act}} = 28$ active protons and $N_{\text{act}} = 38$ active neutrons inside the valence space.

Pairing gaps for the lowest one-quasiparticle states can be calculated from the three-point formulas (20) and (21). Using experimental proton and neutron separation energies obtained from [10], these values are 1.351 MeV for the neutron-odd mother nucleus ^{115}Cd and 1.445 MeV for the proton-odd daughter nucleus ^{115}In.

The calculated Woods-Saxon single-particle energies of the reference nucleus ^{114}Cd are presented in the second column of Table 3. When the scaling constant values $g_{\text{pair}}^{(p)} = 1.130$ and $g_{\text{pair}}^{(n)} = 0.974$ were used to account for the pairing gaps, the resulting unadjusted BCS low-energy one-quasiparticle spectrums can be seen in Figures 2 and 3. The comparison of the proton spectrum to the experimental low-energy level scheme of ^{115}In shows a poor match. Both $\pi 1p_{1/2}$ (0.899 MeV) and $\pi 1p_{3/2}$ (2.279 MeV) are far from their expected energy levels at 0.336 MeV and 0.579 MeV. In the case of neutron orbitals the BCS calculation seems to be able to reproduce the correct set of low-lying one-quasiparticle states at roughly correct energies. The only shortcoming is the wrong order of the states $\nu 0h_{11/2}$ and $\nu 1d_{3/2}$.

In order to match the lowest three proton and neutron one-quasiparticle states with the low-lying states of ^{115}In and ^{115}Cd, some manual adjustments were made to the single-particle energies of Table 3. The proton state $1p_{3/2}$ was raised to -10.71 MeV and the state $0g_{9/2}$ lowered to -10.20 MeV. In the case of neutron orbitals the state $1d_{3/2}$ was raised to -6.71 MeV and the state $0h_{11/2}$ lowered to -6.60 MeV. The new adjusted BCS spectrums with scaling constant values $g_{\text{pair}}^{(p)} = 1.018$ and $g_{\text{pair}}^{(n)} = 0.941$ are likewise presented in Figures 2 and 3.

The reference nucleus ^{114}Cd is a mid-shell nucleus whose quadrupole vibrator level structure is clearly seen in the low-energy part of its level spectrum (see for example Figure 4 and the discussion in [11]). Most noticeably, there are the one-phonon quadrupole singlet 2^+ at 0.558 MeV and the two-phonon quadrupole triplet $0^+, 2^+, 4^+$ at 1.135...1.284 MeV. Furthermore, it is expected to find the three-phonon quadrupole quintet including the states 0^+, 2^+, 3^+, 4^+ and 6^+ at energies about three times that of the one-phonon singlet. The quintet states 0^+, 3^+ and 6^+ are easily

Table 3: The Woods–Saxon single-particle energies for the reference nucleus ^{114}Cd. The calculated single-particle energies are given in the second colomn. If any adjustments to these values were made the adjusted energy is given in the third colomn.

Proton	ϵ_{WS} (MeV)	Adjusted energy (MeV)
$0f_{7/2}$	-16.661358	
$0f_{5/2}$	-12.650281	
$1p_{3/2}$	-11.882409	-10.71
$1p_{1/2}$	-10.325647	
$0g_{9/2}$	-9.3491039	-10.20
$0g_{7/2}$	-3.2118855	
$1d_{5/2}$	-3.8272991	
$2s_{1/2}$	-1.5048858	
$1p_{3/2}$	-1.0081092	
$0h_{11/2}$	-1.5645671	
Neutron	ϵ_{WS} (MeV)	Adjusted energy (MeV)
$0f_{5/2}$	-17.785376	
$1p_{3/2}$	-17.238335	
$1p_{1/2}$	-15.932652	
$0g_{9/2}$	-13.748294	
$0g_{7/2}$	-8.6589794	
$1d_{5/2}$	-9.3609343	
$2s_{1/2}$	-7.5244145	
$1d_{3/2}$	-7.0101843	-6.71
$0h_{11/2}$	-6.0039434	-6.60
$0h_{9/2}$	0.94621968	
$1f_{7/2}$	-1.8642871	
$1f_{5/2}$	0.95156252	
$2p_{3/2}$	-0.83545411	
$2p_{1/2}$	-0.13775468	
$0i_{13/2}$	1.9958558	

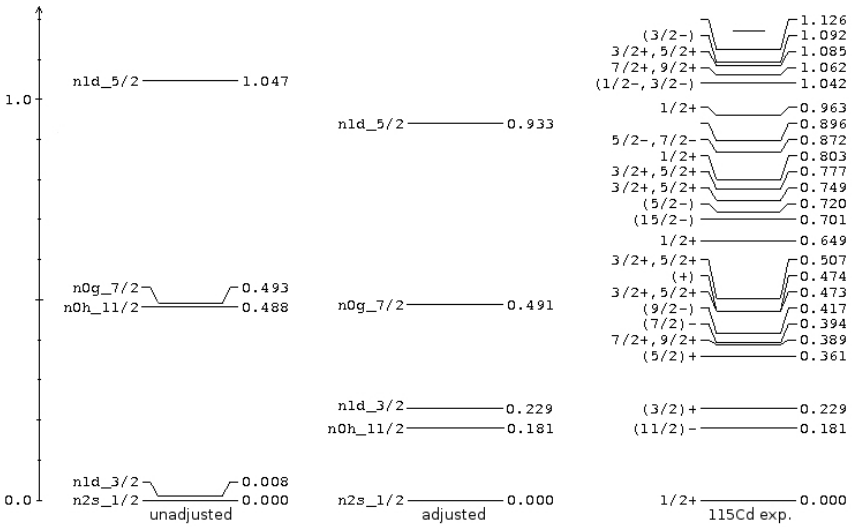

Figure 2: The unadjusted and adjusted BCS spectrums for ^{115}Cd. The Woods–Saxon single-particle energies for the unadjusted spectrum are taken from the second column of Table 3. For the adjusted spectrum the energies of the single-particle orbitals $1d_{3/2}$ and $0h_{11/2}$ were replaced with the values given in the third column of Table 3. The calculated BCS spectrums are compared to the experimental low-energy spectrum of ^{115}Cd.

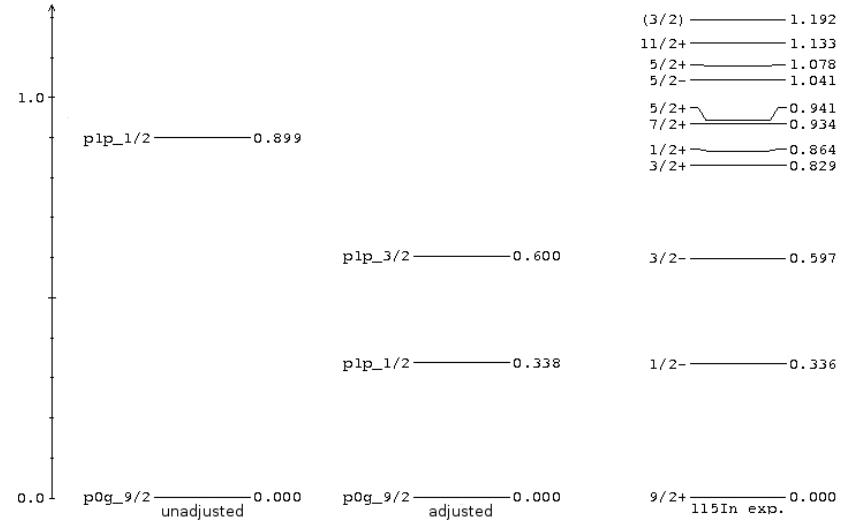

Figure 3: The unadjusted and adjusted BCS spectrums for ^{115}In. The Woods–Saxon single-particle energies for the unadjusted spectrum are taken from the second column of Table 3. The third one-quasiparticle state is $1p_{3/2}$ and it can be found at 2.279 MeV. For the adjusted spectrum the energies of the single-particle orbitals $1p_{3/2}$ and $0g_{9/2}$ were replaced with the values given in the third column of Table 3. The calculated BCS spectrums are compared to the experimental low-energy spectrum of ^{115}In.

Table 4: The QRPA scaling constant values for the multipoles 0^+, 3^-, 4^+ and 5^-.

J^π	g_{pp}	g_{ph}
0^+	0.40	0.40
3^-	1.00	0.74
4^+	1.00	0.96
5^-	1.00	0.76

identified but for the states 2^+ and 4^+ there seem to be several candidates at that energy range. The state 3^- at 1.958 MeV is a possible candidate for the one-phonon octupole singlet state.

Because the QRPA formalism can only deal with one-phonon excitations the two-phonon and three-phonon states fall outside the scope of the theoretical tools that are used in this text. A problematic part of the ^{114}Cd low-energy level scheme are also the additional 0^+ and 2^+ states that are found above the quadrupole triplet. According to [11] these intruder states result from proton excitations across the $Z = 50$ major shell.

The most important QRPA phonons in actual MQPM calculations are the low-energy ones. The effects arising from the high-lying phonons are small and good convergence for the MQPM calculations can generally be established even when the high-energy phonons are neglected altogether. A practical way of implementing this exclusion, and thus lightening the computational burden, is the introduction of an energy cutoff that defines the upper limit for the energies of the QRPA phonons that are to be included in the calculations. For the purposes of this work the adopted energy cutoff was 3.0 MeV.

The scaling constants that were used to fit the multipoles 0^+, 3^-, 4^+ and 5^- below the adopted energy cutoff are given in Table 4. The lowest-energy state of each 3^-, 4^+ and 5^- multipole were fitted close to their proposed experimental companions using only the parameter g_{pp}. In the case of 0^+ it was desirable to adjust also the second lowest state and therefore both the scaling parameters were used. The adopted values $g_{\mathrm{pp}} = 0.40$ and $g_{\mathrm{ph}} = 0.40$ made it possible to keep the 0^+_1 state at the vicinity of the ground-state, while at the same time to lift the 0^+_2 state close to an experimentally confirmed 0^+ state at 2.438 MeV. The state 0^+_1 was omitted in the MQPM calculations since it is known to be completely spurious [12].

It should be noted that the lowest 1^- QRPA state is naturally contaminated by a spurious centre-of-mass motion of the nucleus [2]. To avoid these unwanted effects from affecting the results, the 1^-_1 state was also omitted in the MQPM calculations.

The vibrational characters of the reference nucleus ^{114}Cd are a clear indication that the best fit for the 2^+_1 state is the first excited state at 0.558 MeV. Because the second lowest 2^+ state can likewise naturally be found from the low-energy part of level scheme, it seems almost a necessity to find a good fit also for this state. To cover all the experimentally confirmed 2^+ states near that energy region a systematic way to explore the different options was adopted. The scaling parameter values given in Table 5 can be used to fit the state 2^+_2 to five different energy levels. An experimental 2^+ state can be found at the vicinity of each of these levels.

Table 5: The QRPA scaling constant values for the multipole 2^+. The variations in the values allow the state 2_2^+ to be fitted to different energies while keeping the lower-energy state 2_1^+ close to the quadrupole singlet at 0.558 MeV.

$E(2_2^+)$ (MeV)	g_{pp}	g_{ph}
1.856	1.39	0.66
2.057	1.28	0.68
2.269	1.14	0.70
2.517	0.93	0.72
2.627	0.81	0.73

Neglecting the omitted 0_1^+ state, the calculations involved a total of two 0^+ QRPA states within the energy range from 0 to 3.0 MeV. For each multipole 4^+, 5^-, 6^+ and 8^+ there were likewise two states, but only one state for each 1^+, 3^-, 6^- and 7^-. Depending on the fit of the 2_2^+ state there was a total of three or four 2^+ states below the energy cutoff. For all the other multipoles not mentioned in Tables 4 or 5 the default values $g_{\mathrm{pp}} = 1.00$ and $g_{\mathrm{ph}} = 1.00$ were used for the scaling parameters.

The resulting QRPA spectrums are given in Figure 4. The MQPM spectrums based on these QRPA fits are given in Figures 5 and 6.

The β^- decay scheme of ^{115}Cd is given in Figure 7. In addition to the transitions that come from the ground-state of ^{115}Cd, it is also possible to study transitions from the metastable first excited state $11/2^+$. For the purposes of this text only the transitions with experimentally measured branching probabilities were taken into account. Counting in the order of increasing final state energy, these included the transitions $1/2^- \to 1/2^-$, $3/2^-$, $3/2^+$, $1/2^+$, $5/2^-$ and $11/2^- \to 9/2^+_{g.s.}$, $7/2^+$, $11/2^+$, $13/2^+$.

Figure 5 shows that in every time the first two excited states of ^{115}Cd are found at just the right energy range. In the case of ^{115}In (see Figure 6) the general trend would seem to be that the relevant higher excited states are lying closer to the ground state $9/2^+$ than they should. The only exceptions to this are the theoretical companions to the states $3/2^+$ at 0.829 MeV and $1/2^+$ at 0.864 MeV. The lowest $3/2^+$ state is found at energies around 1.60 MeV and the lowest $1/2^+$ state at energies just over 2 MeV. The lift of the 2_1^+ phonon results in slight changes in the energies of the excited states. Most noticeably the order of excited states $3/2^-$ and $7/2^+$ can be corrected by fitting the 2_1^+ phonon to the highest energy level 2.627 MeV. The downside of this is that the low-energy states $1/2^-$ and $3/2^-$ now decend to lower energies.

Based on the MQPM wave functions, the ^{115}In low-energy states $9/2^+_{g.s.}$, $1/2^-$ and $3/2^-$ are mainly proton-quasiparticle states $\pi 0\mathrm{g}_{9/2}$, $\pi 1\mathrm{p}_{1/2}$ and $\pi 1\mathrm{p}_{3/2}$. At higher energies the states are mainly characterized by their three-quasiparticle components. The largest component for the lowest $3/2^+$ and $1/2^+$ states is $\pi 0\mathrm{g}_{9/2} \oplus 4_1^+$. For the lowest $7/2^+$, $11/2^+$ and $13/2^+$ states this is $\pi 0\mathrm{g}_{9/2} \oplus 2_1^+$. In contrast to these the largest component for the lowest $5/2^-$ state is $\pi 1\mathrm{p}_{3/2} \oplus 2_1^+$. Additional, less significant contributions to these wave functions come mainly from the components $\pi 0\mathrm{g}_{9/2} \oplus 2_2^+$, 4_2^+, 6_1^+, 8_1^+. In the case of ^{115}Cd both the relevant low-energy states $1/2^+_{g.s.}$ and $11/2^-$ are mainly neutron-quasiparticle states $\nu 2\mathrm{s}_{1/2}$ and $\nu 0\mathrm{h}_{11/2}$.

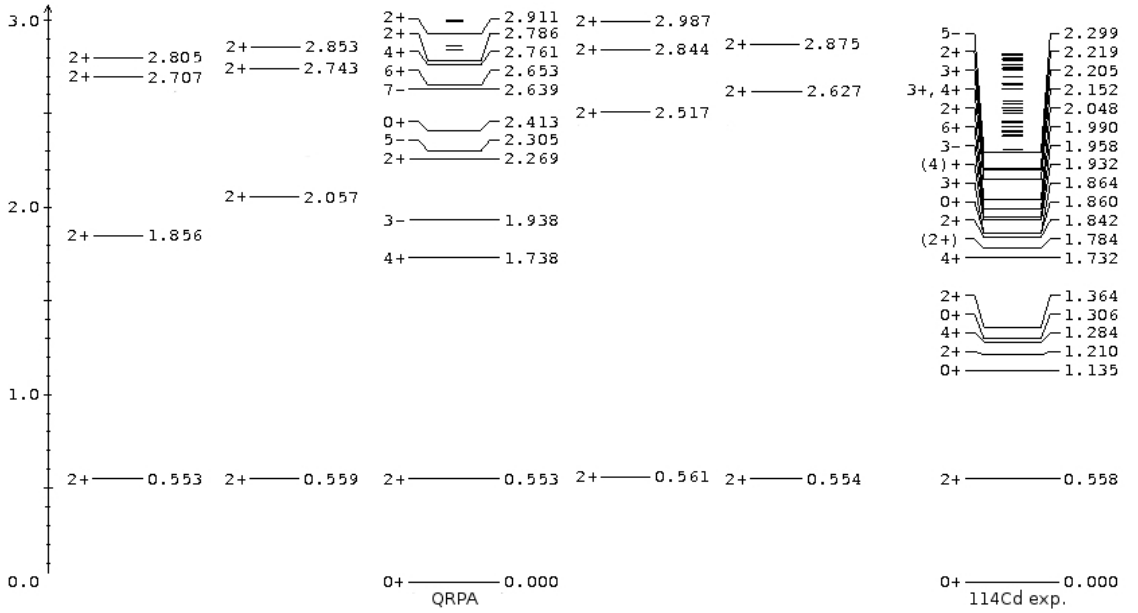

Figure 4: The QRPA spectrums with the state 2_2^+ fitted at five different energy levels from 1.856 MeV to 2.627 MeV. Complete low-energy QRPA level scheme is given only for the fit with $E(2_2^+) = 2.269$ MeV. For all the others only the states of the 2^+ multipole are shown in the figure. The QRPA fits can be compared with the experimental low-energy spectrum of ^{114}Cd on the right.

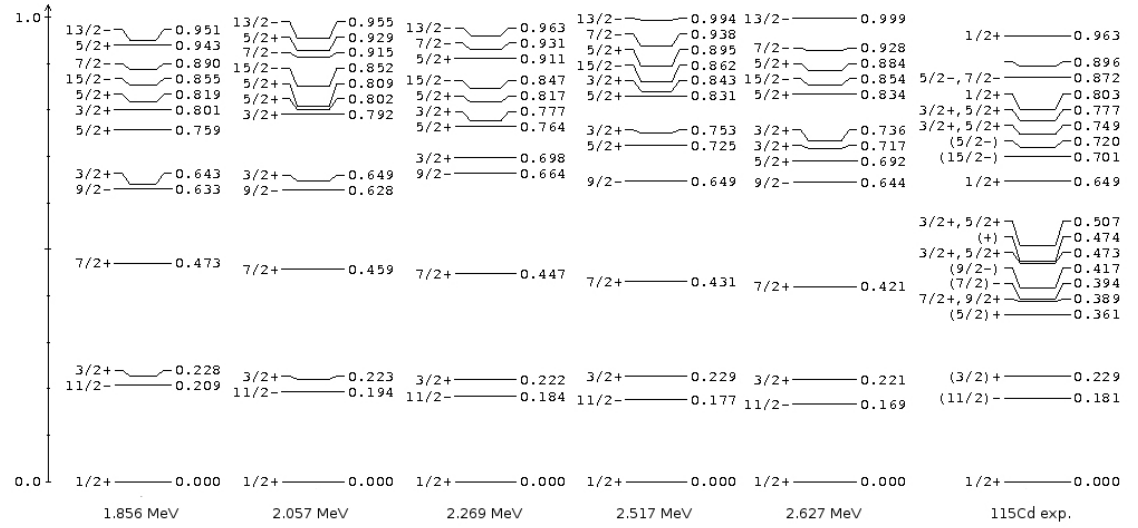

Figure 5: The MQPM spectrums of ^{115}Cd corresponding to the QRPA phonon fits with the state 2_2^+ at five different energy levels from 1.856 MeV to 2.627 MeV. The calculated spectrums can be compared with the experimental low-energy spectrum of ^{115}Cd on the right.

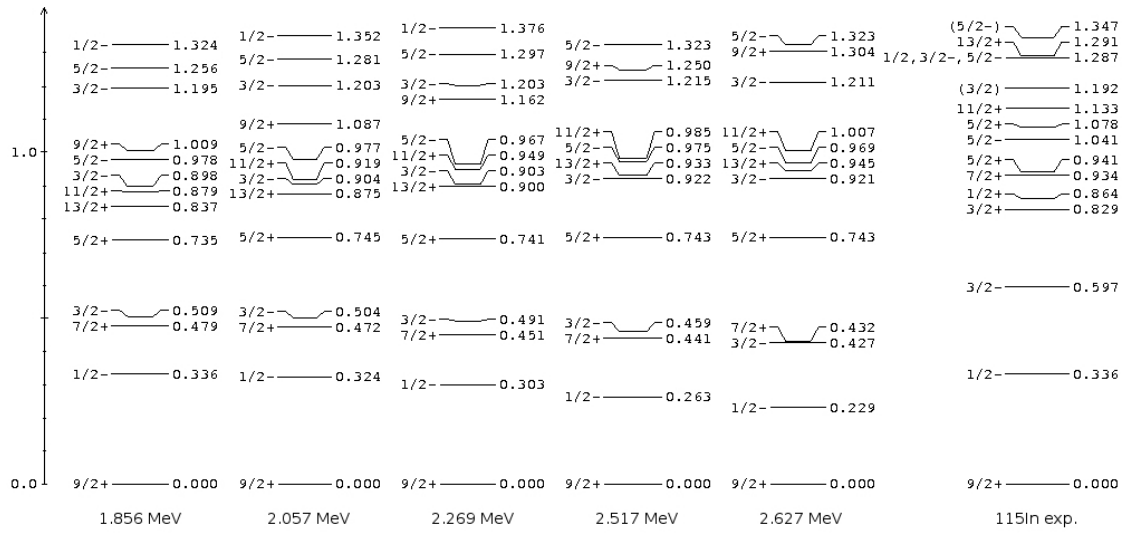

Figure 6: The MQPM spectrums of ^{115}In corresponding to the QRPA phonon fits with the state 2_2^+ at five different energy levels form 1.856 MeV to 2.627 MeV. In each case the lowest $1/2^+$ state is found at just over 2.0 MeV. The lowest $3/2^+$ state is found at 1.571 MeV, 1.579 MeV, 1.590 MeV, 1.603 MeV and 1.607 MeV, respectively for the five different spectrums shown in the figure. The calculated spectrums can be compared with the experimental low-energy spectrum of ^{115}In on the right.

The most interesting features of the MQPM results (see Figure 6) are the large energy discrepancies between the lowest theoretical and experimental $1/2^+$ states. The poor match suggests the state $1/2^+$ to be strongly characterized by its five-quasiparticle components and hence lying beyond the MQPM description. Because of this shortcoming the Fermi transition $1/2^+ \to 1/2^+$ is omitted in the following discussion on the transition half-lives. Judging by the match between the lowest theoretical and experimental $3/2^+$ states, it should be taken into consideration that these discrepancies might likewise arise from the strong five-quasiparticle components. This time however the effect does not seem to be quite that severe.

The needed transition Q-values are given in Table 6. Also shown are the branching probabilities that can be used to calculate the experimental partial half-lives displayed in Table 7. Using the CCTDs calculated from the MQPM results the theoretical partial half-lives of these transitions are given in Table 7. Corresponding to the chosen five QRPA phonon fits there are accordingly a total of five different sets of calculated half-lives. The results collected in Table 7 are also shown in the graphs of Figure 8.

The uncertainties regarding the structure of the ^{114}Cd state 4^+ at 1.732 MeV make it compelling to study the effect of fitting the QRPA phonon 4_1^+ to higher energies. After neglecting the 4^+ state at 1.932 MeV due to its presumed quadrupole three-phonon structure the next possibility is the state $3^+, 4^+$ at 2.152 MeV. There is also a experimentally confirmed 4^+ state at 2.391 MeV. Using a scaling constant value $g_{\rm ph} = 0.78$ for the 4^+ multipole, the QRPA phonon state 4_1^+ can be raised to 2.156 MeV.

Going through the same different options to fit the state 2_2^+ as in the above discussion, i.e. using all the parameter values given in Table 5, another set of QRPA results

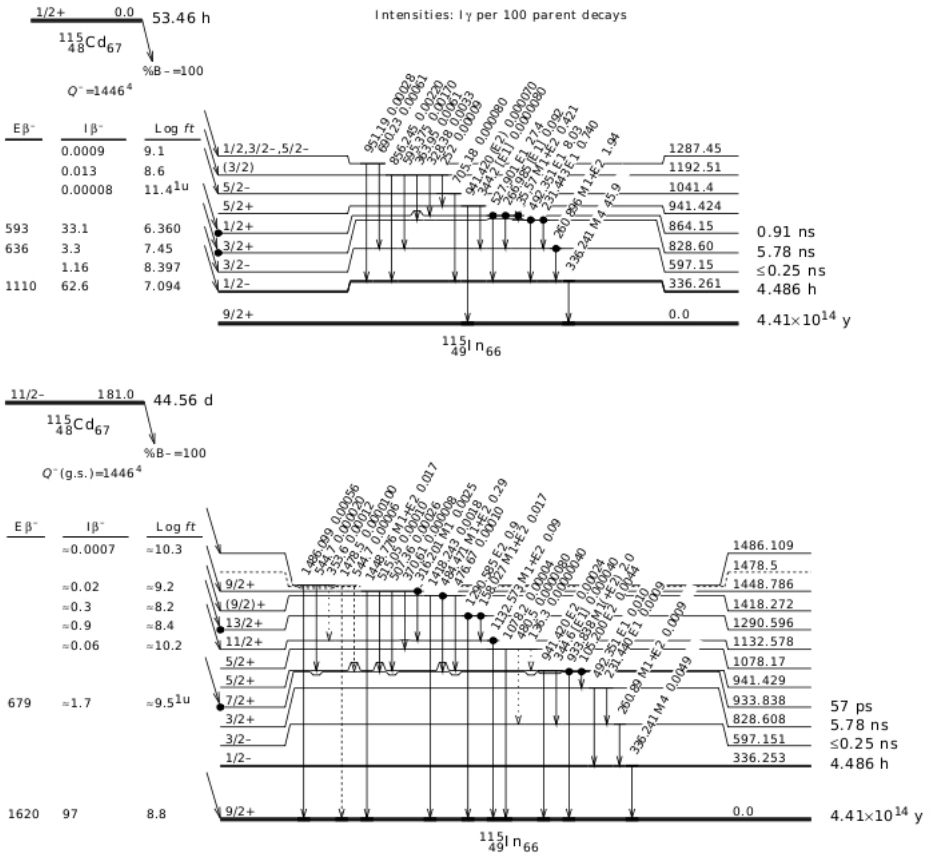

Figure 7: The β^- decay scheme of ^{115}Cd. Shown here are the experimentally measured branching probabilities and logft-values for the various transitions that come from the ground-state $1/2^+$ and the first excited state $11/2^-$. Also given is experimentally confirmed γ decay information.

Table 6: The transition Q-values are calculated from the experimental results of the level scheme of Figure 7. Also shown is the branching probability and the forbiddenness of the given transition. The notation 1u means that the transition is first forbidden unique.

Initial state $(J^\pi)_i = 1/2^+_{g.s.}$ (0.0 MeV)				
$(J^\pi)_f$	E^*_f (MeV)	Q-value (MeV)	I_{β^-} (%)	Forbiddenness
$1/2^-$	0.3363	1.1097	62.6	1
$3/2^-$	0.5972	0.8486	1.16	1
$3/2^+$	0.8286	0.6174	3.3	0
$1/2^+$	0.8642	0.5818	33.1	0
$5/2^-$	1.0414	0.4046	0.00008	1u

Initial state $(J^\pi)_i = 11/2^-$ (0.181 MeV)				
$(J^\pi)_f$	E^*_f (keV)	Q-value (MeV)	I_{β^-} (%)	Forbiddenness
$9/2^+_{g.s.}$	0.0	1.6270	97	1
$7/2^+$	0.9338	0.6932	1.7	1u
$11/2^+$	1.1326	0.4944	0.06	1
$13/2^+$	1.2906	0.3364	0.9	1

Table 7: The sets of β^- decay partial half-lives based on the calculated MQPM results. The first set of values in the third column corresponds to the QRPA results with $E(2^+_2) = 1.856$ MeV, the second set of values in the fourth column to the results with $E(2^+_2) = 2.057$ MeV and so forth. The experimental partial half-lives are calculated from the branching probabilities of Table 6.

Initial state $(J^\pi)_i = 1/2^+_{g.s.}$ (0.0 MeV)						
$(J^\pi)_f$	$t^{(exp)}_{1/2}$	Theoretical partial half-life $t_{1/2}$				
$1/2^-$	3.56 d	15.62 d	13.57 d	11.27 d	8.96 d	7.71 d
$3/2^-$	192.03 d	128.05 d	125.27 d	16.38 d	9.60 d	1.07 d
$3/2^+$	67.50 d	27.75 min	34.96 min	3.27 h	1.31 h	13.51 h
$5/2^-$	7628.42 a	1079.95 a	4220.04 a	51.03 a	1202.63 a	54.14 a

Initial state $(J^\pi)_i = 11/2^-$ (0.181 MeV)						
$(J^\pi)_f$	$t^{(exp)}_{1/2}$	Theoretical partial half-life $t_{1/2}$				
$9/2^+_{g.s.}$	45.94 d	3.17 h	3.05 h	2.96 h	2.90 h	2.79 h
$7/2^+$	7.18 a	1344.49 a	29434.6 a	1277 a	547.96 a	477.57 a
$11/2^+$	203.47 a	9.65 a	1.02 a	1.10 a	38.67 a	10.09 a
$13/2^+$	13.56 a	18.54 a	14.64 a	11.60 a	1.41 a	17.30 a

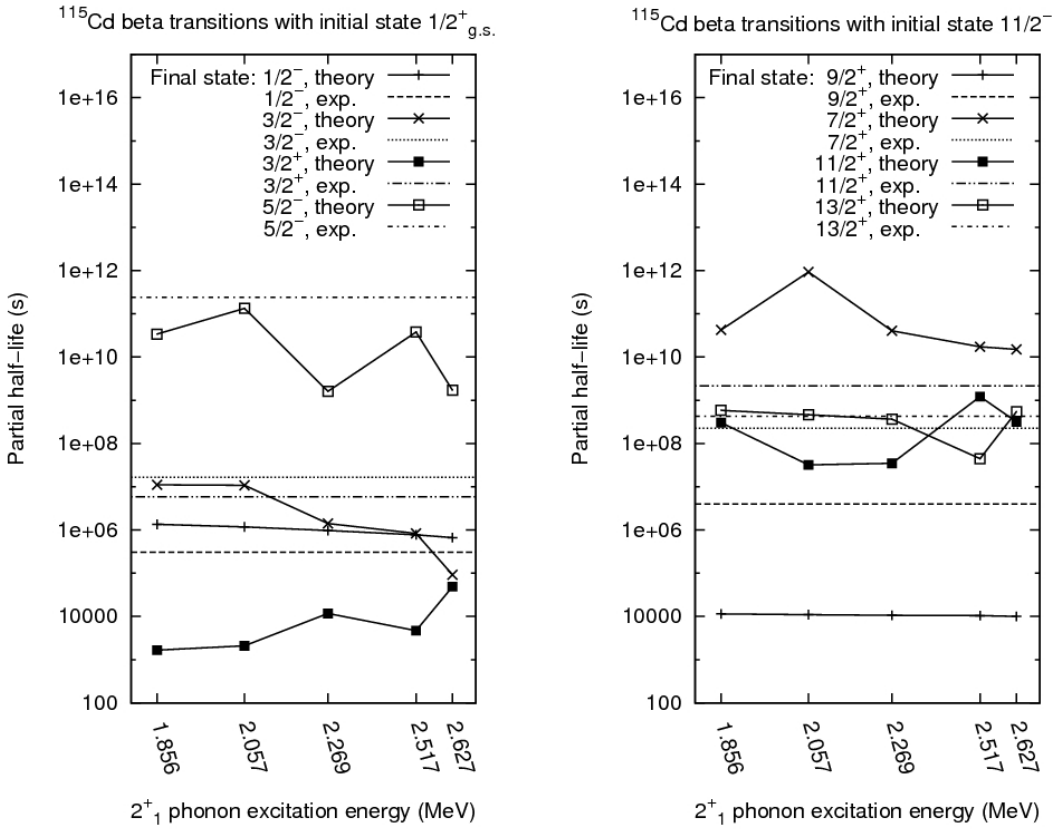

Figure 8: Partial half-lives of Table 7. The values in the left graph are for transitions with initial state $(J^\pi)_i = 9/2^+_{g.s.}$ (0.0 MeV) and the values in the right graph for transitions with initial state $(J^\pi)_i = 11/2^-$ (0.181 MeV). Solid lines connect the calculated theoretical half-life values of a given transition. Dashed lines represent the experimental partial half-lives.

is obtained from the calculations. The low-energy phonon spectrums corresponding to these are exactly the ones given in Figure 4 except for the state 4^+_1 at 2.156 MeV. The MQPM spectrums based on the new QRPA fits are given in Figures 9 and 10.

The new MQPM spectrums of Figures 9 and 10 show in general only slight changes to the previous results. The most noticeable change occures in the excitations energy of the lowest ^{115}In state $3/2^+$ that is now above 2 MeV. The order of the ^{115}Cd low-energy excitation states is corrected when the 2^+_2 phonon energy is lifted to its highest value. However, this happens again at the expence of lowered excitation energies of the low-energy states $1/2^-$ and $3/2^-$.

The calculated theoretical partial half-lives obtained from these MQPM results are given in Table 8 and in Figure 11. Corresponding to the five QRPA phonon fits there are again a total of five different sets of calculated half-lives. The Fermi transition $1/2^+ \rightarrow 1/2^+$ is again omitted. Mean values for the results of Tables 7 and 8 are given in Table 9.

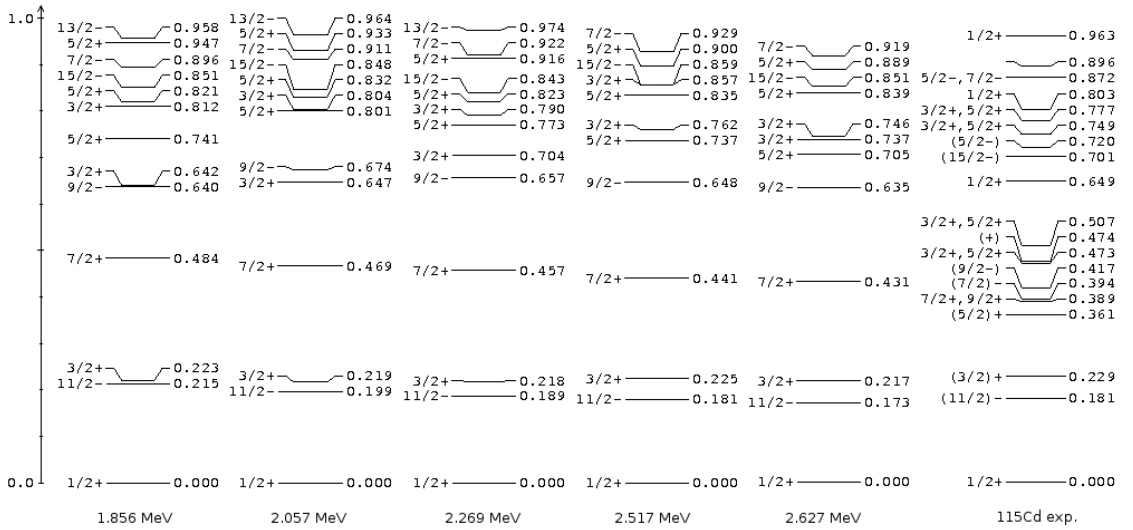

Figure 9: The MQPM spectrums of ^{115}Cd based on the QRPA calculations, where the state 4_1^+ raised to 2.156 MeV. The results correspond to the fits with the state 2_2^+ at five different energy levels from 1.856 MeV to 2.627 MeV. The calculated spectrums can be compared with the experimental low-energy spectrum of ^{115}Cd on the right.

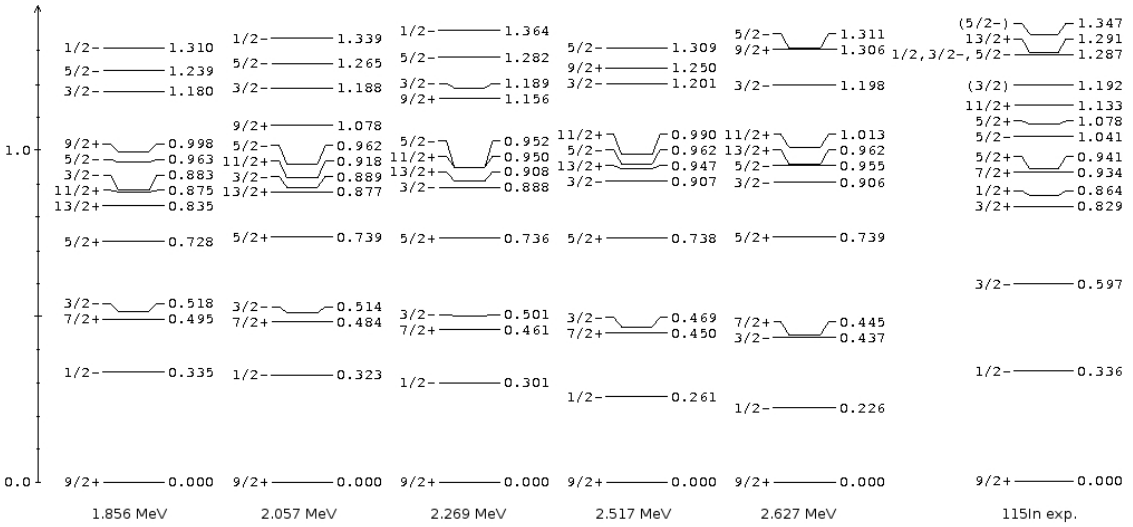

Figure 10: The MQPM spectrums of ^{115}Cd based on the QRPA calculations, where the state 4_1^+ raised to 2.156 MeV. The results correspond to the fits with the state 2_2^+ at five different energy levels from 1.856 MeV to 2.627 MeV. In each case the lowest $1/2^+$ state is found at around 2.5 MeV. The lowest $3/2^+$ state is found at 2.042 MeV, 2.050 MeV, 2.061 MeV, 2.075 MeV and 2.079 MeV, respectively for the five different spectrums shown in the figure. The calculated spectrums can be compared with the experimental low-energy spectrum of ^{115}In on the right.

Table 8: The new sets of β^- decay partial half-lives based on the calculated MQPM results with the QRPA state 4_1^+ fitted to 2.156 MeV. The first set of values in the third column corresponds to the QRPA results with $E(2_2^+) = 1.856$ MeV, the second set of values in the fourth column to the results with $E(2_2^+) = 2.057$ MeV and so forth. The experimental partial half-lives are calculated from the branching probabilities of Table 6.

Initial state $(J^\pi)_i = 1/2^+_{g.s.}$ (0.0 MeV)						
$(J^\pi)_f$	$t_{1/2}^{(exp)}$	Theoretical partial half-life $t_{1/2}$				
$1/2^-$	3.56 d	15.63 d	13.48 d	11.16 d	8.87 d	7.62 d
$3/2^-$	192.03 d	138.71 d	128.86 d	17.77 d	11.25 d	1.06 d
$3/2^+$	67.50 d	202.04 d	1.05 h	55.52 min	56.44 min	264.09 d
$5/2^-$	7628.42 a	2933.82 a	4998.63 a	50.69 a	4816.72 a	11258 a

Initial state $(J^\pi)_i = 11/2^-$ (0.181 MeV)						
$(J^\pi)_f$	$t_{1/2}^{(exp)}$	Theoretical partial half-life $t_{1/2}$				
$9/2^+_{g.s.}$	45.94 d	2.81 h	2.67 h	2.55 h	2.43 h	2.30 h
$7/2^+$	7.18 a	1406.43 a	1336.39 a	29064.3 a	1288.34 a	462.16 a
$11/2^+$	203.47 a	13.79 a	316.24 d	334.12 d	177.65 a	11.62 a
$13/2^+$	13.56 a	22.94 a	18.14 a	1.07 a	1.33 a	2.57 a

Table 9: The mean values of the calculated partial half-lives. The values in the third column are the mean values for the results of Table 7. Those in the fourth colomn are the mean values for the results of Table 8.

Initial state $(J^\pi)_i = 1/2^+_{g.s.}$ (0.0 MeV)			
$(J^\pi)_f$	$t_{1/2}^{(exp)}$	Average theoretical $t_{1/2}$	
$1/2^-$	3.56 d	(11.4 ± 1.5) d	(11.4 ± 1.5) d
$3/2^-$	192.03 d	(60 ± 30) d	(60 ± 40) d
$3/2^+$	67.50 d	(4 ± 3) h	(90 ± 60) d
$5/2^-$	7628.43 a	(1300 ± 800) a	(5000 ± 2000) a

Initial state $(J^\pi)_i = 11/2^-$ (0.181 MeV)			
$(J^\pi)_f$	$t_{1/2}^{(exp)}$	Average theoretical $t_{1/2}$	
$9/2^+_{g.s.}$	45.94 d	(178 ± 4) min	(153 ± 6) min
$7/2^+$	7.18 a	(7000 ± 6000) a	(7000 ± 6000) a
$11/2^+$	203.47 a	(12 ± 7) a	(40 ± 40) a
$13/2^+$	13.56 a	(13 ± 4) a	(9 ± 5) a

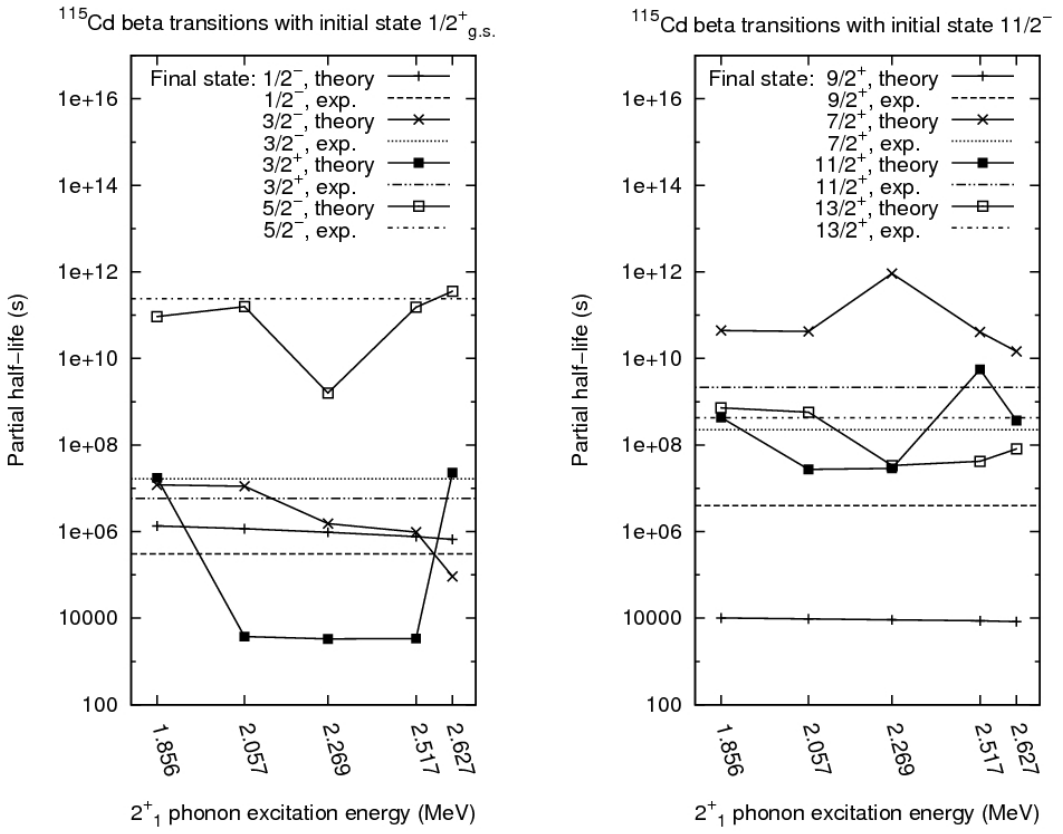

Figure 11: The partial half-lives of Table 8. The values in the left graph are for transitions with initial state $(J^\pi)_i = 9/2^+_{g.s.}$ (0.0 MeV) and the values in the right graph for transitions with initial state $(J^\pi)_i = 11/2^-$ (0.181 MeV). Solid lines connect the calculated theoretical half-life values of a given transition. Dashed lines represent the experimental partial half-lives.

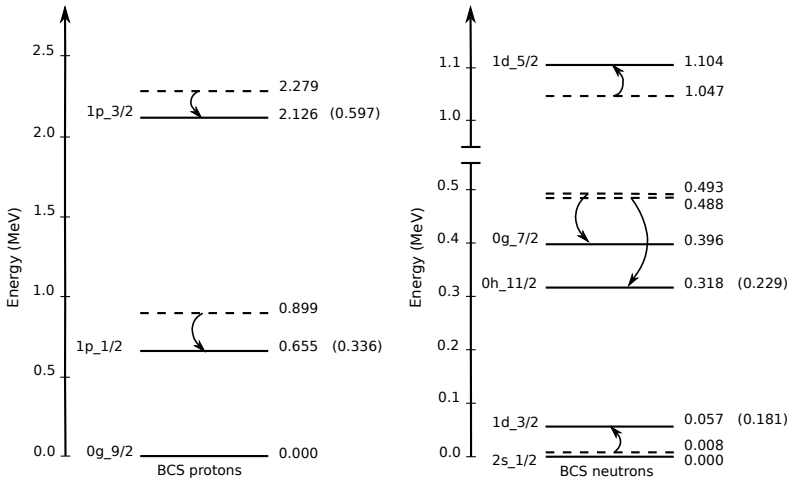

Figure 12: The BCS spectrums showing the effects of increasing the spin-orbit interaction strength from $1.00\,v_{\rm LS}^0$ to $1.08\,v_{\rm LS}^0$. Dashed lines indicate the energy levels for $1.00\,v_{\rm LS}^0$ (see Figures 2 and 3) and the solid ones for $1.08\,v_{\rm LS}^0$. Values inside the parentheses are the experimentally confirmed energies for the relevant low-energy states. In either case, no adjustments were made to the Woods–Saxon single-particle energies. For $1.08\,v_{\rm LS}^0$ the scaling constant values $g_{\rm pair}^{(p)} = 1.115$ and $g_{\rm pair}^{(n)} = 0.949$ were used to account for the pairing gaps.

3.2 Calculations with adjusted spin-orbit interaction strength

As a further exercise the effect of adjusting the spin-orbit interaction strength was also examined. The needed small adjustment were done simply by multiplying the interaction strength v_{LS}^0 of Eq. (7) by a constant close to a unity. As depicted in Figure 12 the increase in the interaction strength tends to bring the low-lying proton one-quasiparticle states closer together. Also the neutron one-quasiparticle states $0{\rm h}_{11/2}$ and $1{\rm d}_{3/2}$ are shifted towards their proper experimental companions.

The BCS spectrums with adjusted Woods-Saxon single-particle energies for spin-orbit interaction strengths $0.92\,v_{\rm LS}^0$, $0.96\,v_{\rm LS}^0$, $1.04\,v_{\rm LS}^0$ and $1.08\,v_{\rm LS}^0$ are given in Figures 14 and 15. The goal was to fit the low-energy one-quasiparticle states in the same way as in the adjusted BCS spectrums of Figures 2 and 3 which were taken to be the reference fits with $1.00\,v_{\rm LS}^0$. To archieve this the new sets of single-particle energies for the orbitals listed in Table 3 and the scaling constants $g_{\rm pair}^{(p)}$ and $g_{\rm pair}^{(n)}$ had to be adjusted slightly differently each time. The dependence of the single-particle energies on the spin-orbit interaction strength is depicted in the graphs of Figure 13. The manual adjustments that were made to the energies of the relevant orbitals are given in Table 10. The scaling constants that were used to account for the pairing gaps are given in the same table.

In the case of QRPA phonons the fit with $E(2_2^+) = 2.517$ MeV and $E(4_1^+) = 2.156$ MeV was chosen as the reference with $1.00\,v_{\rm LS}^0$. Again the goal was to fit the phonons in the same way as in this reference fit. This required that each time a slightly different sets of scaling constants $g_{\rm pp}$ and $g_{\rm ph}$ had to be used. The scaling constants for multipoles 0^+ and 2^+ are given in Table 11. For all the other multipoles essentially the same constants were used as in the Table 4. The resulting QRPA spectrums are given in Figure 16. The MQPM spectrums corresponding to them are given in Figures 17 and 18.

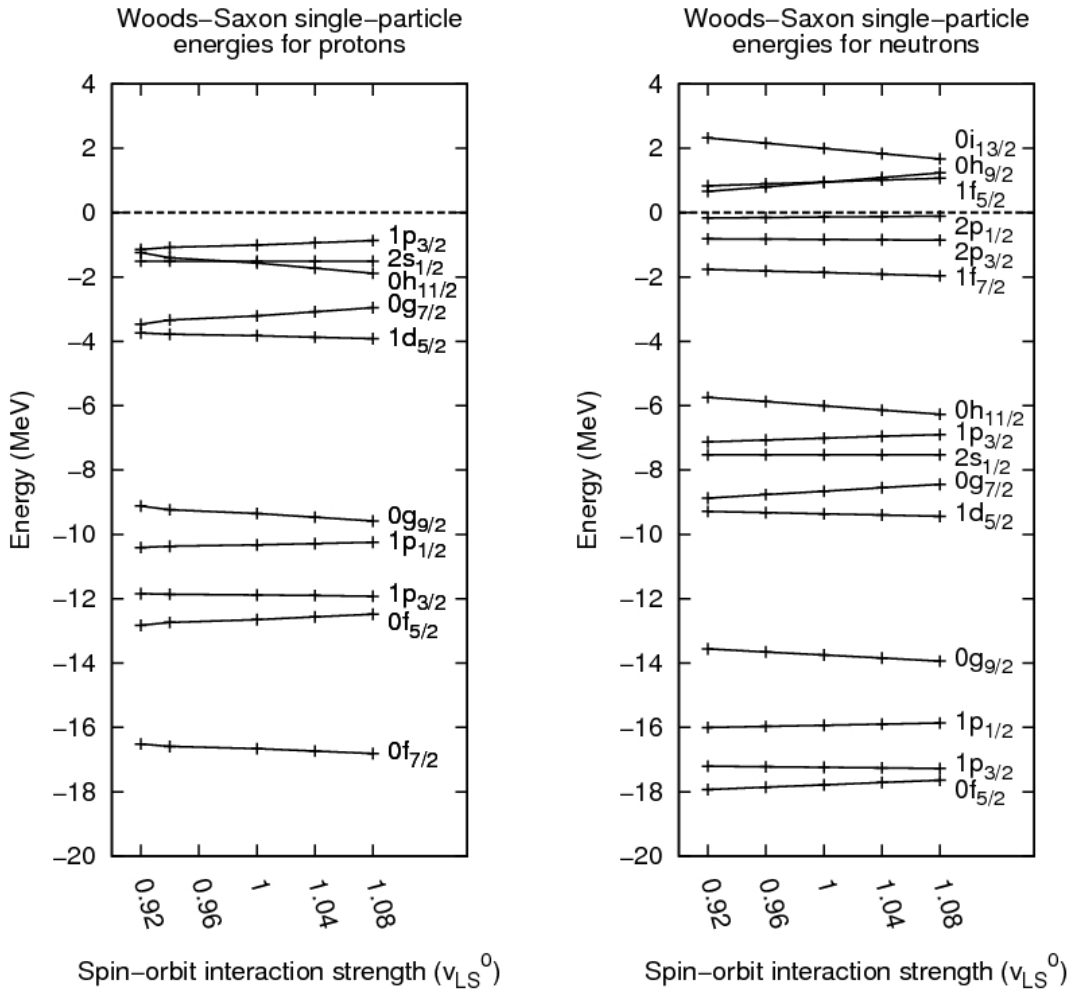

Figure 13: The Woods–Saxon single-particle energies for the valence space orbitals of the reference nucleus ^{114}Cd. The actual values corresponding to the spin-orbit interaction strength $1.00\,v_{\rm LS}^0$ are the unadjusted energies given in Table 3.

Table 10: The proposed manual adjustments to the Woods–Saxon single-particle energies of the proton orbitals $1p_{3/2}$ and $0g_{9/2}$ and the neutron orbitals $1d_{3/2}$ and $0h_{11/2}$. Also given are the scaling constants used to account for the pairing gaps of the mother and daughter nucleus. The reference case with $1.00\,v_{\rm LS}^0$ corresponds to the choices made earlier in Chapter 3.1.

Interaction strength	Adjusted $\epsilon_{\rm WS}$ (MeV)				Scaling constants	
	$\pi 1p_{3/2}$	$\pi 0g_{9/2}$	$\nu 1d_{3/2}$	$\nu 0h_{11/2}$	$g_{\rm pair}^{(p)}$	$g_{\rm pair}^{(n)}$
$0.92\,v_{\rm LS}^0$	-10.79	-10.20	-6.79	-6.64	1.019	0.943
$0.96\,v_{\rm LS}^0$	-10.75	-10.24	-6.75	-6.62	1.019	0.942
$1.00\,v_{\rm LS}^0$	-10.71	-10.20	-6.71	-6.60	1.018	0.941
$1.04\,v_{\rm LS}^0$	-10.67	-10.16	-6.66	-6.57	1.018	0.941
$1.08\,v_{\rm LS}^0$	-10.62	-10.12	-6.60	-6.53	1.016	0.941

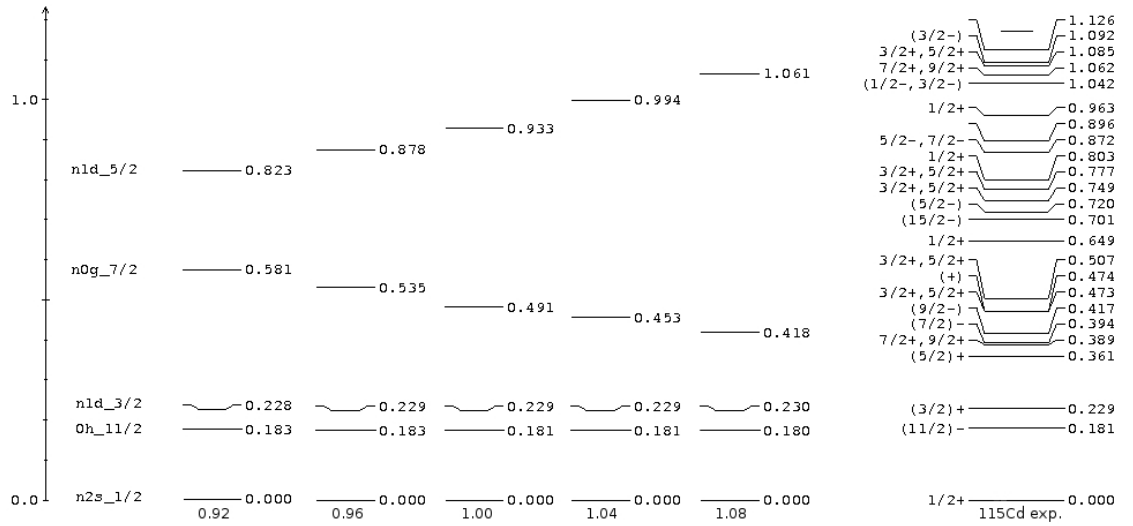

Figure 14: The BCS spectrums of ^{115}Cd with the spin-orbit interaction strength varied from $0.92\,v^0_{\rm LS}$ to $1.08\,v^0_{\rm LS}$. The spectrum with $1.00\,v^0_{\rm LS}$ is the same adjusted one as in Figure 2. The calculated spectrums can be compared with the experimental low-energy spectrum of ^{115}Cd on the right.

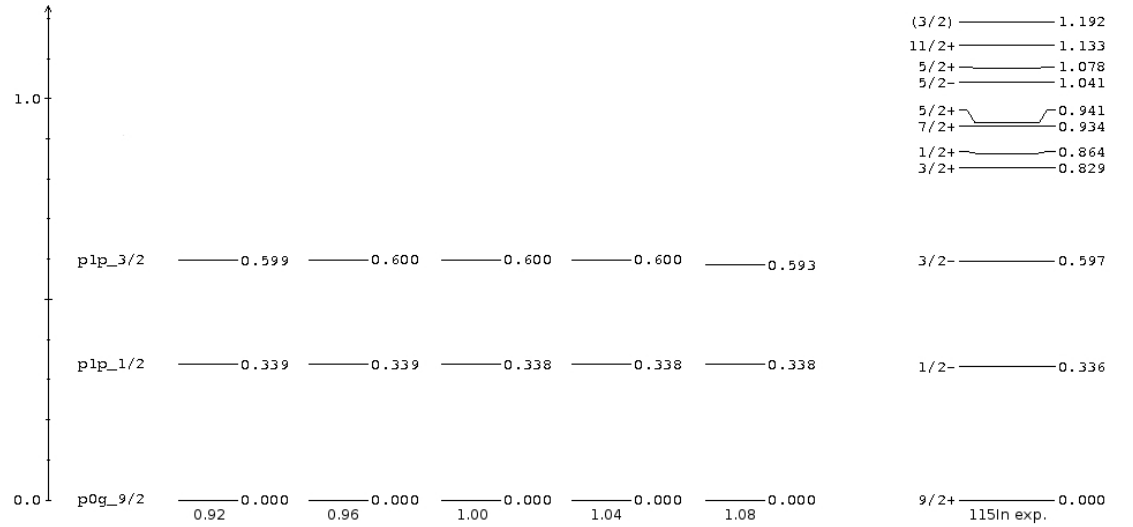

Figure 15: The BCS spectrums of ^{115}In with the spin-orbit interaction strength varied from $0.92\,v^0_{\rm LS}$ to $1.08\,v^0_{\rm LS}$. The spectrum with $1.00\,v^0_{\rm LS}$ is the same adjusted one as in Figure 3. The calculated spectrums can be compared with the experimental low-energy spectrum of ^{115}In on the right.

Table 11: The QRPA scaling constants for multipoles 0^+ and 2^+. The adopted values correspond to the QRPA fit of Chapter 3.1 with $E(2_2^+) = 2.517$ MeV and $E(4_1^+) = 2.156$ MeV.

Interaction strength	Multipole 0^+		Multipole 2^+	
	g_{pp}	g_{ph}	g_{pp}	g_{ph}
$0.92\, v_{\mathrm{LS}}^0$	0.50	0.40	0.93	0.73
$0.96\, v_{\mathrm{LS}}^0$	0.46	0.40	0.87	0.73
$1.00\, v_{\mathrm{LS}}^0$	0.40	0.40	0.93	0.72
$1.04\, v_{\mathrm{LS}}^0$	0.35	0.40	0.89	0.72
$1.08\, v_{\mathrm{LS}}^0$	0.30	0.40	0.96	0.71

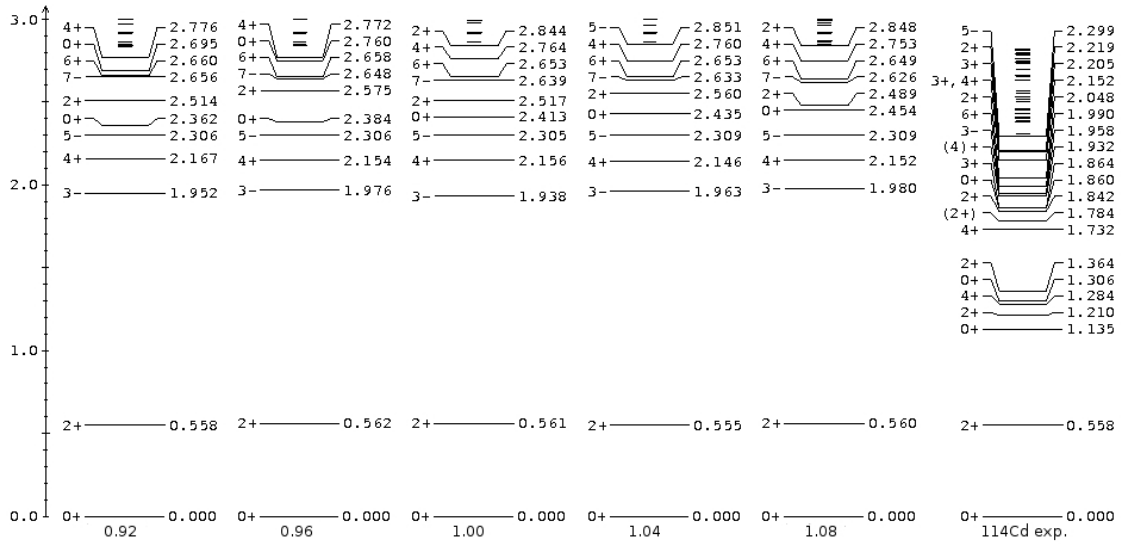

Figure 16: The QRPA spectrums based on the BCS calculations of Figures 14 and 15. The reference spectrum with spin-orbit interaction strength $1.00\, v_{\mathrm{LS}}^0$ is the QRPA fit of Chapter 3.1 with $E(2_2^+) = 2.517$ MeV and $E(4_1^+) = 2.156$ MeV.

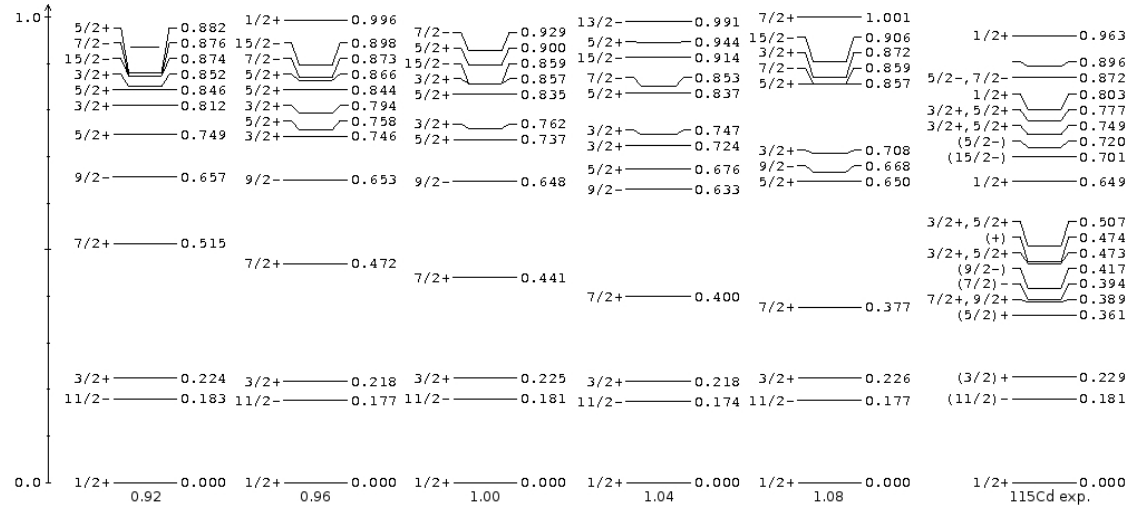

Figure 17: The MQPM spectrums of ^{115}Cd that correspond to the QRPA phonon fits of Figure 16. The reference spectrum with spin-orbit interaction strength $1.00\, v^0_{\rm LS}$ is one in Figure 9 with $E(2^+_2) = 2.517$ MeV. The calculated spectrums can be compared with the experimental low-energy spectrum of ^{115}Cd on the right.

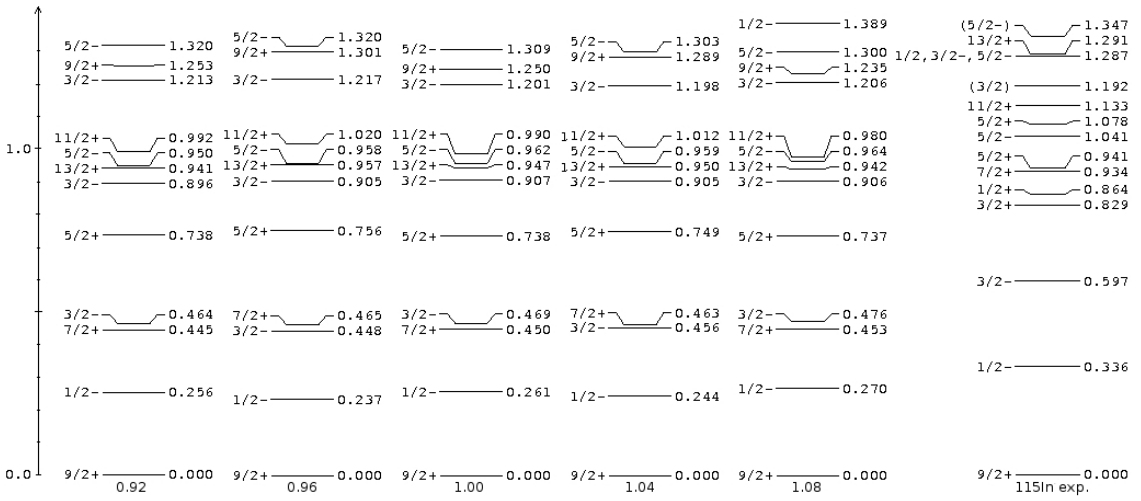

Figure 18: The MQPM spectrums of ^{115}In that correspond to the QRPA phonon fits of Figure 16. The reference spectrum with spin-orbit interaction strength $1.00\, v^0_{\rm LS}$ is one in Figure 10 with $E(2^+_2) = 2.517$ MeV. In each case the lowest $1/2^+$ state is found at around 2.5 MeV. The lowest $3/2^+$ state is found at 2.082 MeV, 2.066 MeV, 2.075 MeV, 2.062 MeV and 2.073 MeV, respectively for the five different spectrums shown in the figure. The calculated spectrums can be compared with the experimental low-energy spectrum of ^{115}Cd on the right.

Table 12: The sets of β^- decay partial half-lives based on the calculated MQPM results of Figures 17 and 18. The reference set in the fifth column with spin-orbit interaction strength $1.00\,v_{\mathrm{LS}}^0$ is taken from Table 8. The experimental partial half-lives are calculated from the branching probabilities of Table 6.

Initial state $(J^\pi)_i = 1/2^+_{g.s.}$ (0.0 MeV)						
$(J^\pi)_f$	$t_{1/2}^{(exp)}$	Theoretical partial half-life $t_{1/2}$				
		$0.92\,v_{\mathrm{LS}}^0$	$0.96\,v_{\mathrm{LS}}^0$	$1.00\,v_{\mathrm{LS}}^0$	$1.04\,v_{\mathrm{LS}}^0$	$1.08\,v_{\mathrm{LS}}^0$
$1/2^-$	3.56 d	7.88 d	7.78 d	8.87 d	8.80 d	10.36 d
$3/2^-$	192.03 d	14.68 d	1.11 d	11.25 d	1.19 d	10.63 d
$3/2^+$	67.50 d	1.22 h	4.29 a	56.44 min	1.95 a	4.29 h
$5/2^-$	7628.42 a	29870.8 a	8122.1 a	4816.72 a	1999.1 a	2338.62 a

Initial state $(J^\pi)_i = 11/2^-$ (0.181 MeV)						
$(J^\pi)_f$	$t_{1/2}^{(exp)}$	Theoretical partial half-life $t_{1/2}$				
		$0.92\,v_{\mathrm{LS}}^0$	$0.96\,v_{\mathrm{LS}}^0$	$1.00\,v_{\mathrm{LS}}^0$	$1.04\,v_{\mathrm{LS}}^0$	$1.08\,v_{\mathrm{LS}}^0$
$9/2^+_{g.s.}$	45.94 d	2.45 h	2.34 h	2.43 h	2.46 h	2.56 h
$7/2^+$	7.18 a	2605.09 a	494.68 a	1288.34 a	647.85 a	817.74 a
$11/2^+$	203.47 a	3.02 a	5.33 a	177.65 a	7.76 a	1.32 a
$13/2^+$	13.56 a	1.09 a	1.58 a	1.33 a	2.03 a	1.40 a

Figures 17 and 18 show that changes to the previous results are again only slight. In each case the lowest $3/2^+$ and $1/2^+$ states that should correspond to the low-energy ones found at around 0.85 MeV are above 2 MeV. The theoretical partial half-lives calculated using this yet another set of MQPM results are given in Table 12 and in Figure 19. Mean values for the calculated results are given in Table 13.

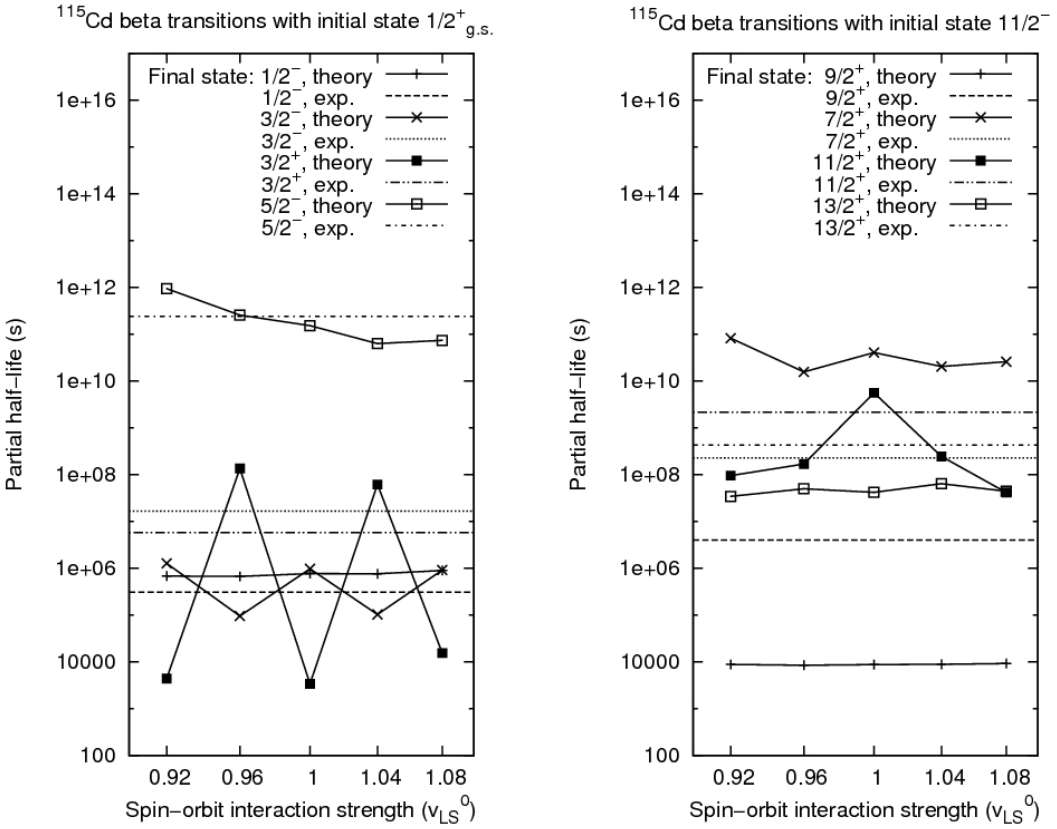

Figure 19: The partial half-lives of Table 12. The values in the left graph are for transitions with initial state $(J^\pi)_i = 9/2^+_{g.s.}$ (0.0 MeV) and the values in the right graph for transitions with initial state $(J^\pi)_i = 11/2^-$ (0.181 MeV). Solid lines connect the calculated theoretical half-life values of a given transition. Dashed lines represent the experimental partial half-lives.

Table 13: The mean values of the calculated partial half-lives of Table 12.

Initial state $(J^\pi)_i = 1/2^+_{g.s.}$ (0.0 MeV)		
$(J^\pi)_f$	$t_{1/2}^{(exp)}$	Average theoretical $t_{1/2}$
$1/2^-$	3.56 d	(8.7 ± 0.5) d
$3/2^-$	192.03 d	(8 ± 3) d
$3/2^+$	67.50 d	(1.2 ± 0.8) a
$5/2^-$	7628.43 a	(9000 ± 6000) a

Initial state $(J^\pi)_i = 11/2^-$ (0.181 MeV)		
$(J^\pi)_f$	$t_{1/2}^{(exp)}$	Average theoretical $t_{1/2}$
$9/2^+_{g.s.}$	45.94 d	(147 ± 3) min
$7/2^+$	7.18 a	(1200 ± 400) a
$11/2^+$	203.47 a	(40 ± 40) a
$13/2^+$	13.56 a	(1.5 ± 0.2) a

4 Conclusions

In this master's thesis the beta decay of ^{115}Cd was studied using microscopic quasiparticle-phonon model. The three-quasiparticle spectrums obtained from application of the MQPM formalism are presented in Chapter 3. The main results of this work are the calculated partial half-lives for the various β^- transitions. These theoretical estimates are given in Tables 7, 8, and 12 of Chapter 3.

The examination of the calculated partial half-lives of Tables 7 and 8 show that in several cases a value roughly of the same order of magnitude with the experimental one can be found. However, in many cases the closest values must be picked from different sets of results. It is therefore difficult to point out a single set of values that as a whole gives the best agreement with experiments. Furthermore, for some transitions the discrepancies between the theoretical and the experimental values seem be to systematically very large.

The differences between the values listed in Tables 7 and 8 result from the QRPA fits that affect the wave functions of the relevant excitation states. It can be seen that for some transitions the half-lives depend rather smoothly on the excitation energy of the QRPA state 2_2^+. In other cases on the other hand, the effects are much more unpredictable and can cause significant amounts of variation to the half-life values. The significance of the QRPA state 4_1^+ seems to likewise vary largely from one transition to another.

Based on the transition half-lives, the most problematic transitions seem to be $11/2^- \rightarrow 9/2^+_{g.s.}$ and $11/2^- \rightarrow 7/2^+$, where the calculated results systematically differ considerably from the experimental values. The Gamow–Teller transition $1/2^+ \rightarrow 3/2^+$ is also a disappointment. However, in this case it must be noted that the final state $3/2^+$ is very poorly matched with its experimental companion at 0.829 MeV. As stated in Chapter 3, this might be due to the strong five-quasiparticle components in the wave function of the state. Even though it is reasonable to expect somewhat less accurate results because of this shortcoming, the large variations in the half-life values seem nevertheless very unpredictable.

The mean values of Table 9 smooth out the variation in the half-life values but in reality this is not a drastic improvement over the separate sets of results. Only for few transitions the actual, experimentally deduced partial half-life can be found to lie inside the standard error margins of the mean value. Because of the large variation in the half-life values, these errors tend get likewise very large. It must be noted that here the whole consept of mean value is perhaps a bit vague. Rather than being a statistical problem, the differing sets of partial half-lives result in this case only from the fact that there is no certainty of how exactly the QRPA states should be arranged. In any case it would seem that the high-energy fit of the 4_1^+ phonon is a more appropriate choice over the low-energy one.

The other part of Chapter 3 concerned the study of changing the spin-orbit interaction strength. The conclusion based on the calculated partial half-lives of Table 12 is that although the increase of the interaction strength improved the BCS one-quasiparticle spectrum, the agreement between theoretical and experimental half-lives as a whole is not any better. To be able to study the effects that result solely from the spin-orbit interaction strength, it must be ensured that the BCS and QRPA spectrums resemble all the time closely to some pre-selected reference fits. Because

slightly different parameter values and adjustments had to be chosen, it was difficult to keep the spectrums to look exactly the same. Hence it is possible that other factors could have also affected the results.

One spesific feature of the results is that the partial half-lives for the transition $11/2^- \rightarrow 9/2^+_{g.s.}$ are shifted hardly at all. This stability can be explained by the one-quasiparticle structures of the states $11/2^-$ and $9/2^+_{g.s.}$ that leaves them largely unaffected by the QRPA fits. Large discrepancies between the theoretical and the experimental values must result from the failure of the theoretical formalism to properly descripe both or either one of these states. Because most of the ^{115}In three-quasiparticle states have a structure, where the one-quasiparticle state $9/2^+_{g.s.}$ is combined with the low-energy QRPA phonons the above argument is likely to explain many of the problems encountered with the other transitions also. As already stated in Chapter 3, a particulary noticeable feature of the ^{115}In MQPM spectrums is that in general the relevant excited states seem to lie closer to the ground state than they should.

One possible way to investigate the effect of the ground state $9/2^+_{g.s.}$ could be to try to explore the different options of adjusting the Woods–Saxon single-particle energies that affect the BCS quasiparticle spectrums. In practice this seems to be method of trial and error because beforehand there is no clear indication of what the proper adjustments need to be.

References

[1] J. Toivanen, J. Suhonen, *Microscopic quasiparticle-phonon description of odd-mass $^{127-133}$Xe isotopes and their β decay*, Phys. Rev. C57 (1998) 1237

[2] J. Suhonen, *From Nucleons to Nucleus: Concepts of Microscopic Nuclear Theory*, Springer, Berlin, 2007

[3] K. Kolinde, Phys. Rep. 68 (1981) 121

[4] D. J. Rowe, *Equations-of-Motion Method and Extended Shell Model*, Rev. Mod. Phys. 40 (1968) 153

[5] M. T. Mustonen, M. Aunola, J. Suhonen, *Theoretical description of the fourth-forbidden non-unique β decay of ^{113}Cd and ^{115}In*, Phys. Rev. C73 (2006) 054301

[6] E. Ydrefors, M. T. Mustonen, J. Suhonen, *MQPM description of the structure and beta decays of the odd A = 95, 97 Mo and Tc isotopes*, Nuclear Physics A 842 (2010) 33-47

[7] H. Behrens, W. Buhring, *Electron Radial Wave Functions and Nuclear Beta-decay*, Clarendon Press, Oxford, 1982

[8] K. S. Krane, *Introductory Nuclear Physics*, John Viley & Sons, 1988

[9] F. Halzen, A. D. Martin, *Quarks and Leptons: An introductory Course in Modern Particle Physics*, John Viley & Sons, 1984

[10] National Nuclear Data Center, http://www.nndc.bnl.gov/

[11] S. W. Yates, *Probing multiphonon excitations in nearly spherical nuclei with fast neutrons*, J. Phys. G: Nucl. Part. Phys. 31 (2005) S1393-S1397

[12] M. Baranger, Phys. Rev. 120 (1960) 957